AD-A143 612 INFLUENCE OF CONTAINER INTERACTIONS ON THE VAPORIZATION 1/1
THERMODYNAMICS OF NICKEL(U) MATERIALS RESEARCH LABS
ASCOT VALE (AUSTRALIA) P L MART MAY 83 MRL-R-884

UNCLASSIFIED F/G 11/6 NL

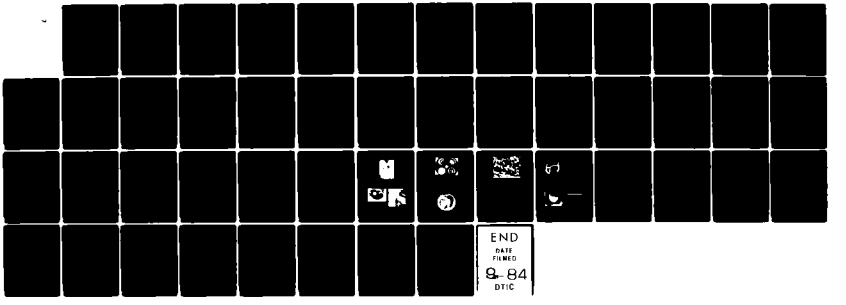

END
DATE FILMED
8-84
DTIC

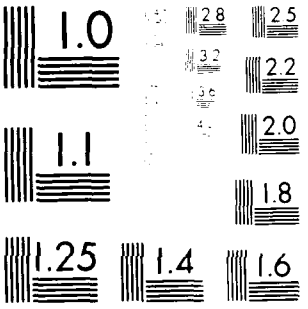

(12)

DEPARTMENT OF DEFENCE

DEFENCE SCIENCE AND TECHNOLOGY ORGANISATION

MATERIALS RESEARCH LABORATORIES

MELBOURNE, VICTORIA

REPORT

MRL-R-884

INFLUENCE OF CONTAINER INTERACTIONS ON THE VAPORIZATION THERMODYNAMICS OF NICKEL

Peter L. Mart

Approved for Public Release

DEPARTMENT OF DEFENCE

MATERIALS RESEARCH LABORATORIES

REPORT

MRL-R-884

INFLUENCE OF CONTAINER INTERACTIONS ON THE VAPORIZATION THERMODYNAMICS OF NICKEL

Peter L. Mart

ABSTRACT

This report describes studies to determine the nature of the interactions between nickel and various refractory containers encountered in high-temperature Knudsen cell vaporization systems. High-temperature mass spectrometric measurements, in conjunction with metallographic studies, were used to determine how these interactions influenced the vaporization thermodynamics of nickel. Such information is essential to permit the determination of valid high-temperature thermodynamic activity data in multi-component alloy systems.

The studies revealed that graphite is an unsuitable container for molten nickel. Due to a substantial solubility of graphite in nickel, under these circumstances the nickel activity and its enthalpy of vaporization are significantly reduced in comparison to pure nickel. Recrystallized alumina and stabilized zirconia refractories did not react with molten nickel, but only zirconia was stable towards the molybdenum and tungsten Knudsen cell jackets.

Recommendations are made for suitable containers for studies of the thermodynamic properties of nickel-aluminium and nickel-aluminium-platinum alloys. These alloy systems are important because they constitute the aluminide protective coatings applied to hot end components of military gas turbines.

POSTAL ADDRESS: Director, Materials Research Laboratories
P.O. Box 50, Ascot Vale, Victoria 3032, Australia

DOCUMENT CONTROL DATA SHEET

REPORT NO.	AR NO.	REPORT SECURITY CLASSIFICATION
MRL-R-884	AR-003-295	UNCLASSIFIED

TITLE

INFLUENCE OF CONTAINER INTERACTIONS ON THE VAPORIZATION THERMODYNAMICS OF NICKEL

AUTHOR(S)

Peter L. MART

CORPORATE AUTHOR
Materials Research Laboratories
P.O. Box 50,
Ascot Vale, Victoria 3032

REPORT DATE	TASK NO.	SPONSOR
MARCH 1983	DST 82/129	DSTO

CLASSIFICATION/LIMITATION REVIEW DATE	CLASSIFICATION/RELEASE AUTHORITY
	Superintendent, MRL Metallurgy Division

SECONDARY DISTRIBUTION

Approved for Public Release

ANNOUNCEMENT

Announcement of this report is unlimited

KEYWORDS

Nickel	Thermodynamics	Effusion
Vaporizing	Enthalpy	Refractories
	Mass Spectroscopy	Molten
	Knudsen cell	

COSATI GROUPS 0702

ABSTRACT

This report describes studies to determine the nature of the interactions between nickel and various refractory containers encountered in high-temperature Knudsen cell vaporization systems. High-temperature mass spectrometric measurements, in conjunction with metallographic studies, were used to determine how these interactions influenced the vaporization thermodynamics of nickel. Such information is essential to permit the determination of valid high-temperature thermodynamic activity data in multi-component alloy systems.

The studies revealed that graphite is an unsuitable container for molten nickel. Due to a substantial solubility of graphite in nickel, under these circumstances the nickel activity and its enthalpy of vaporization are significantly reduced in comparison to pure nickel. Recrystallized alumina and stabilized zirconia refractories did not react with molten nickel, but only zirconia was stable towards the molybdenum and tungsten Knudsen cell jackets.

Recommendations are made for suitable containers for studies of the thermodynamic properties of nickel-aluminium and nickel-aluminium-platinum alloys. These alloy systems are important because they constitute the aluminide protective coatings applied to hot end components of military jet turbines.

CONTENTS

CONTENTS

INFLUENCE OF CONTAINER INTERACTIONS ON THE VAPORIZATION THERMODYNAMICS OF NICKEL

1. INTRODUCTION

Basic thermodynamic properties of high-temperature alloys are of fundamental importance to our understanding of their behaviour under operational conditions. Because of the lack of reliable thermodynamic data, the development of structural superalloys and protective coatings used in the fabrication of components in gas turbine engines has proceeded somewhat empirically, and there is little doubt that the development has been inefficient.

One of the Tasks of High Temperature Properties (HTP) Group, Task No. DST 82/129 entitled "High Temperature Properties of Metals", has as its objectives:

(1) to carry out basic research into the thermodynamic, kinetic and mechanistic aspects of high-temperature degradative phenomena such as oxidation and hot corrosion in metals and alloys of current and potential relevance to the Australian Defence Force; and

(2) to investigate and develop methods whereby the high-temperature corrosion resistance of such metals and alloys can be enhanced.

To facilitate the study of high-temperature thermodynamics, a rotatable, four-compartment Knudsen cell (quad-cell) has been developed at MRL as an effusion source for the mass spectrometric study of high temperature systems. In a previous report [1] of the thermodynamic properties of the nickel-aluminium system, using the quad-cell mass spectrometry technique, difficulties were reported with the containment of liquid aluminium and aluminium-rich alloys. This prevented the determination of aluminium activities, but nickel activities were reported for the high nickel compositions with nickel atom fractions, x_{Ni}, greater than 0.54.

The present study was undertaken as a preliminary to the determination of the activities of both nickel and aluminium over the complete range of compositions.

It is well established [2,3] that vapour pressure measurements by Knudsen cell effusion are very susceptible to interactions between the sample and the container. Where possible, the selection of a chemically inert container is desirable, although a reactive container may be used if a protective layer of reaction products is formed that provides kinetic stability [4,5]. A guide to the suitability of a particular container for metallic alloys is to examine its interaction with the separate components of the alloy. The absence of interaction with the pure elements indicates that reliable thermodynamic properties are likely to be obtainable for the alloys in the same container. Conversely, interaction with either or both of the component elements is likely to prevent the collection of reliable thermodynamic data. If the nature and the extent of the interaction can be well characterized, then it may be possible to correct the thermodynamic data derived for the alloy, but such a procedure is best avoided if a non-interactive system can be found.

Accordingly, a study was made of the interaction of nickel and aluminium with a number of potentially suitable container materials. The present paper primarily reports on the interaction with nickel; results of the investigations into the interaction with aluminium, and the detailed study of the nickel-aluminium alloys, will be reported in a future paper.

There are numerous literature reports on the vaporization thermodynamics of nickel by a variety of techniques, including Knudsen mass effusion, Knudsen effusion mass spectrometry, Langmuir vaporization (both mass loss and mass spectrometry), and gas transport. The earlier work has been reviewed by Hultgren et al. [6] and the value selected for the enthalpy of vaporization of nickel was $\Delta H^{o}_{298} = 430.1 \pm 2.1$ kJ mol^{-1}. This value (calculated by the Third Law method) was based mainly on gas transport measurements. Hultgren et al. disregarded the high values obtained from mass spectrometry because of "the low absolute accuracy of this method" [6]. It should be noted, however, that these were Lamgmuir vaporization mass spectrometry measurements rathen than Knudsen effusion mass spectrometry. Hultgren et al. also considered that the Knudsen mass effusion results of Nesmeyanov and Man [7,8] should be rejected due to the orifice area dependence of the nickel vapour pressures. However Man and Nesmeyanov [8] calculated nickel vapour pressures inconsistent with their observed mass losses. The correct pressures (calculated in the present work from their original results) are approximately two orders of magnitude lower than those they reported, but still about twenty times higher than the accepted literature values [6]. The recalculated pressures produce a mean enthalpy of vaporization (Third Law method) which is significantly higher than than calculated by the authors and also reported by Hultgren et al. [6] in their review.

Rutner and Haury [14] also performed a statistical analysis of literature data on the vapour pressure of nickel, they too rejecting the (incorrect) data of Nesmeyanov and Man [7,8]. They calculated by the Third Law method a best value for the enthalpy of vaporization,

$\Delta H^{\circ}_0 = 424.5 \pm 2.6$ kJ mol^{-1}. Using the enthalpy functions of Hultgren et al. [6] this yields the value $\Delta H^{\circ}_{298} = 426.5 \pm 2.6$ kJ mol^{-1}.

Since non-identical sets of experimental data were analyzed by the above reviewers, the two best values are not strictly comparable. However, they are in agreement within their respective error limits, and for convenience have been averaged to yield the value $\Delta H^{\circ}_{298} = 428.3 \pm 4$ kJ mol^{-1}.

In Table 1 the Knudsen effusion data from these reviews are summarized, together with subsequent literature data. Third Law enthalpies of vaporization of nickel have been calculated from the data of Alcock and Kubik [10], and recalculated from the data of Man and Nesmeyanov [8]. With the exception of the results of the latter authors [7,8], the remaining literature Knudsen effusion data agree reasonably well with the above averaged value for the enthalpy of vaporization of nickel. In particular, the agreement obtained by Knudsen effusion mass spectrometry [12] is satisfactory. This indicates that, with suitable containment, it should be possible to obtain reliable thermodynamic data for nickel using this technique.

TABLE 1. Knudsen Effusion Measurements of the Enthalpy of Vaporization of Nickel

Sample/Cell Material	Method	Temperature	ΔH°_{298} (kJ mol^{-1})	Ref.
Ni/Mo	Mass loss	1400-1527K	341.1 ± 0.8	7
Ni/Mo	Mass loss	1320-1550K	*393.1 ± 4.2	8
Ni/Alumina	Mass loss	1463-1628K	430.0	9
Ni/Alumina	Mass loss	1835-1882K	*429.5 ± 0.3	10
Ni/Alumina	Mass loss and Torsion	1723-1873K	----	11
NiO and Ni/ Alumina	Mass spectrometric	1575-1709K	**425.8 ± 2.0	12
Ni^{63}/Unknown	Mass loss	1440-1600K	421.7 ± 0.3	13

* calculated in this work

** recalculated value [14]

2. EXPERIMENTAL CONSIDERATIONS

2.1 Apparatus

In the present study a multiple Knudsen-cell mass spectrometry technique was used. In this a rotatable four-compartment Knudsen cell (quad-cell), developed at MRL, was the effusion source for a time-of-flight mass spectrometer [15,16].

The schematic diagram of the quad-cell is shown in Fig. 1a. The geometry of the high vacuum chamber, and of the pre-machined refractory metal quad-cells, limited the size of the crucible liners that could be used, which, in turn, limited the ratio of the evaporating surface area to effusion hole area. The internal diameter of the cell compartment was 8 mm, the internal diameter of cell liners was typically 5 mm, and effusion orifice diameter was 1 mm. This lead to ratios of the evaporating surface area (taken as geometrical cross sectional area of the cell) to effusion orifice area of 64 for the cell alone, and 25 for the cell containing a crucible. While the former figure is similar to that used by Ward [2], the latter figure is lower than is desirable (by a factor of four). However, it is generally accepted that the value for the coefficient of vaporization of nickel is close to unity [6], so that equilibrium conditions should have been maintained within the cell even at a lower ratio.

As a result of the initial experiments, a second design of quad-cell was manufactured, as shown in Fig. 1b. In this design the effusion orifice (1 mm diameter) was ultrasonically drilled in the ceramic liner (1.5 mm wall thickness), and the hole in the quad-cell was countersunk such that none of the effusing beam could contact the quad-cell. A ceramic lid was lapped and polished to ensure a good seal to the top of the ceramic liner, thus preventing escape of vapour within the quad-cell.

The choice of electron bombardment heating of the Knudsen cell to attain the high temperatures required (up to 2000K) necessitated that the cells were made of, or surrounded by, electrically conductive materials. This limited the choice of cell materials to the more commonly available refractory metals (tungsten, molybdenum and tantalum), as well as high density graphite. Refractory cell liners of recrystallized alumina and calcia-stabilized zirconia were available in the form of small crucibles, and were also machined from boron nitride and graphite.

2.2 Quad-Cell Selection

2.2.1 Refractory Metal Quad-Cells

Choice of refractory metal crucibles to contain liquid nickel is governed by the mutual solubility of the nickel and refractory metal. Molybdenum, tungsten and tantalum all show substantial solid solubility in nickel [17,18], and are therefore unacceptable as crucibles and quad-cells without liners.

The low values for the enthalpy of vaporization of nickel measured by Nesmeyanov and Man [7,8] may be due to their use of molybdenum Knudsen cells. Chatillon et al. [3] have shown that other 'parasitic' sources may contribute to the molecular beam emitted from the Knudsen cell and sampled by the mass spectrometer. These include climbing of the liquid sample up the cell walls, when the liquid wets the cell material, allowing free evaporation to take place from the external surface surrounding the effusion hole. This non-equilibrium evaporation can cause the sampled flux to be much higher than that due to effusion alone, and may be partly responsible for the erroneously high nickel vapour pressures calculated from the data of Nesmeyanov and Man [7,8]. Surface diffusion of the sample along the cell walls and through the effusion hole can also contribute significantly to the evaporated material [3].

Refractory metals may be suitable for use as quad-cells if the nickel is contained in an inert crucible liner, which will prevent the molten nickel from climbing the cell walls. The possibility still remains for interaction between the nickel vapour and the exposed refractory metal surface (for instance at the effusion hole). The solubility of nickel in molybdenum, tungsten and tantalum is about one atomic percent at 1700K [17,18] and is therefore likely to have little effect on the measured vapour pressure. Notwithstanding the use of inert crucible liners, surface diffusion of nickel may still contribute to the evaporation process and produce erroneously high nickel vapour pressures.

2.2.2 Graphite Quad-Cells

It is known that molten nickel can dissolve substantial amounts of carbon [17], which indicates that graphite crucibles are unlikely to be good containers for nickel. The activity and solubility of carbon in Ni-C alloys has been reported by numerous investigators over the temperature interval 1200-1500K, and these results are critically discussed by Bradley et al. [19]. However, there are no reports on the activity of nickel in liquid nickel saturated with carbon, and there is contention as to the stability of the Ni_3C phase which intersects this liquidus curve [17].

2.2.3 Ceramic Crucibles and Graphite Quad-Cells

Either of the ceramics alumina or zirconia is suitable to contain molten nickel since the free energy of formation of nickel oxide is considerably less than that of the ceramic oxide [20]. However, the interaction between the ceramic crucible and a graphite quad-cell is considerable, as discussed by Jansson [21]. At 1800K in vacuum alumina will react with carbon to form Al_4C_3 via the equation

$$2\ Al_2O_3 + 9\ C \longrightarrow Al_4C_3 + 6CO\ (g) \qquad (1)$$

with pCO = 427Pa. Oxycarbides may also be formed [22]. Similar thermodynamic calculations using the data of Kubaschewski and Alcock [23] indicate that

zirconia will be even more unstable in respect to carbide formation, and the non-stoichiometry of zirconia also permits formation of reduced ZrO_{2-x} with evolution of CO.

2.2.4 Boron Nitride Crucibles and Graphite Quad-Cells

Boron nitride is of marginal suitability as a container for liquid nickel, since it decomposes incongruently to solid boron and gaseous nitrogen at these temperatures. From JANAF thermochemical tables [24] the pressure of nitrogen from this dissociation is quite high (about 10^{-2}Pa) at 2000K, and the boron formed reacts with the nickel to form NiB above 1700K [25]. Furthermore, thermodynamic calculations based on the thermodynamic data of Bockris et al. [26] indicate that boron nitride should be quite unstable with respect to carbon, and react to form boron carbide and nitrogen gas at temperatures as low as 1000K.

2.2.5 Ceramic Crucibles and Refractory Metal Quad-Cells

The thermodynamics of the reaction of alumina and zirconia with the refractory metals molybdenum, tungsten and tantalum has been reported [27,28]. Under a vacuum of 10^{-2}Pa, alumina is equally stable to molybdenum and tungsten with no interaction occurring below about 2200K, while tantalum is fairly unstable and forms gaseous tantalum oxides. Zirconia is slightly more stable than alumina, with no interaction occurring below about 2300K for molybdenum and tungsten, and about 2100K for tantalum. The CaO stabilizing additive in zirconia may react with refractory metals and reduce the reaction resistance of the zirconia ceramic, but the volatility of the CaO ensures that no reaction occurs with molybdenum and tungsten below 2300K [27].

2.2.6 Summary

From the above considerations, it was decided that refractory metal quad-cells used alone would be unsuitable for containing liquid nickel. The use of an inert crucible liner was essential, and the combination of alumina or stabilized zirconia crucibles with molybdenum or tungsten quad-cells seemed worthy of investigation.

In the case of graphite quad-cells, it was decided to check, by experiment, the validity of the thermodynamic considerations, and the possibility of achieving kinetic stability with various crucible liner materials. Accordingly, crucibles fabricated from graphite, alumina, stabilized zirconia and boron nitride were used as liners in graphite quad-cells.

2.3 Materials

Nickel shot of nominal purity 99.95 wt % for Ni was used throughout, and was spectroscopically and chemically analyzed at MRL. It contained 0.06_5

wt % C, ~ 0.06 wt % Si and ~ 0.003 wt % S and ~ 40 ppm Al as the major impurities, with Cu and Zn (both 4 ppm), Mg, Mn and Ag (all 1 ppm) as lesser impurities. Gold powder (99.9 kgc) of 99.99 [illegible] was used for calibration purposes.

2.4 Temperature Measurement

Temperatures of the blackbody holes in the quad-cell were measured with an Ircon model 138P automatic optical pyrometer, or with a Leeds and Northrup model 8627 disappearing filament optical pyrometer. Temperature uniformity measurements were performed as described by Johnston and Burley [16], and vertical and circumferential temperature gradients in the quad-cells were minimised by adjustment of the power input to sections of the two independently controlled heating filaments. While the vertical temperature uniformity in the quad-cell was typically within ± 2K, circumferential temperature gradients varied from ± 5K in molybdenum to ± [illegible] K in graphite quad-cells, for experimental temperatures in the range 1650K to [illegible] K. This variation is considerably greater than that reported [16] by Johnston and Burley (± 1K for molybdenum quad-cells) and is attributed to deterioration of the symmetry of the furnace, particularly the heat shields. Pyrolytic graphite is a better thermal conductor than molybdenum and probably accounts for the greater gradients observed with graphite cells. Although such temperature gradients are undesirable in pressure measurements in multi-compartment Knudsen cells, temperature corrections made by the dynamic back-extrapolation method of Johnston and Burley [16] were applied to correct the measured temperatures for each orifice in turn. Temperatures were also corrected for the transmittance of the window using the expression [17]

$$\frac{1}{T_A} = \frac{1}{T_O} + \frac{\lambda \ln \tau \varepsilon_\lambda}{C_2} \qquad (2)$$

where T_A and T_O are the actual and measured temperatures in kelvin, respectively, τ is the window transmittance (0.62, measured using the Ircon pyrometer and an NBS tungsten strip filament lamp), λ = 0.653 x 10^{-6}m, C_2 = 1.43879 x 10^{-2}mK, and ε_λ is the emittance for light of wavelength λ (ε_λ = 1 for a blackbody).

2.5 Mass Spectrometry

Ion currents were monitored for the $^{58}Ni^+$ isotope (68.3% natural abundance) during nickel vaporization experiments, and for the $^{197}Au^+$ (100%) during gold vaporization experiments to check the calibration of the apparatus. Electron energies of 50 eV and 40 eV were used in the ion source of the mass spectrometer in the first two experiments respectively, thereafter 35 eV was used in all experiments. A regulated trap current of 0.5 mA was used throughout.

Ion currents were corrected for background by subtracting the ion current measured when the effusing beam was directed [illegible]° away from the ion source. This compensated for spurious re-evaporations from the heat shields

and other hot surfaces adjacent to the quad-cell. However, it does not distinguish possible surface-creep of material from the cell orifice; a shutter between the cell and the ion source would be required to achieve this. Such a shutter would increase the distance between the quad-cell and ion source, reducing the amount of effusate entering the ion source, and hence reducing the sensitivity of detection by the mass spectrometer.

2.6 Thermodynamic Calculations

For vaporization of nickel from different crucibles and quad-cells, and for calibration experiments using gold, the enthalpy of vaporization was measured since this provides a clear indication of possible changes in thermodynamic activity of the nickel due to interaction with the container, or changes in the vapour pressure due to temperature nonuniformity.

The second-law enthalpy of vaporization is derived from the expression

$$\Delta H_T = - R \frac{d \ln K_p}{d(\frac{1}{T})} \qquad (3)$$

where K_p is the equilibrium constant for the vaporization reaction and T is the absolute temperature.

Hence

$$\Delta H_T = - R \frac{d \ln P_i}{d(\frac{1}{T})} \qquad (4)$$

where P_i is the equilibrium vapour pressure of species i inside the Knudsen cell. The relationship between this and the mass spectrometric ion current I_i^+ is

$$P_i = k_i I_i^+ T \qquad (5)$$

where k_i is a calibration factor depending on the relative ionization cross section, the gain of the electron multiplier in the mass spectrometer, and the isotope abundance, for the particular isotope of species i being measured. It also includes a geometry-dependent sensitivity factor which is independent of species. The latter factor incorporates the Clausing factor, K_c, which depends on the physical dimensions of the effusion orifice and corrects for the reduced ion intensity due to collisions between the effusing molecules and the orifice walls. While the calibration factor can be calculated, enabling determination of absolute pressures P_i, this is unnecessary in the second-law method.

Thus

$$\Delta H_T = - R \frac{d \ln (I_i^+ T)}{d(\frac{1}{T})} + \text{constant} \qquad (6)$$

ΔH_T is calculated from the slope of a plot of $\ln(I_i^+ T)$ versus $\frac{1}{T}$, and as such

this method [illegible] emphasizes any temperature errors. The standard enthalpy of vaporization, ΔH°_{298}, is then calculated from the expression

$$\Delta H^{\circ}_{298} = \Delta H_T - \Delta(H^{\circ}_T - H^{\circ}_{298}) \quad (7)$$

where $\Delta(H^{\circ}_T - H^{\circ}_{298})$ is the difference in the literature tabulated [6] enthalpy functions for the vapour and condensed phase respectively of the vaporizing species.

The enthalpy of vaporization may also be calculated by the third-law method

$$\Delta H^{\circ}_{298} = -RT\ln K_p + T\Delta \text{ fef} \quad (8)$$

where the change in the free energy function (fef) is given by

$$\Delta \text{ fef} = -\Delta \frac{G^{\circ}_T - H^{\circ}_{298}}{T} \quad (9)$$

Values of fef for nickel and gold are tabulated in the literature [6]. Thus values of ΔH°_{298} are calculated from each experimental point, which is advantageous when the data cover an insufficient temperature range for accurate use of the second-law method. While calculation by both the second- and third-law methods is desirable, in practice it was not experimentally convenient to determine the absolute vapour pressures for each cell and each experimental temperature, as required in the third-law method.

It should be noted that comparison of the measured ion currents, or $\ln(I^{+}_{Ni}T)$ values in the second-law plots, is only possible for compartments of the same quad-cell in the same experiment, where the transmission factors for the effusion orifices have been calibrated. The absolute ion currents will vary from run to run, depending upon changes in the alignment of the effusing molecular beam with the ion source of the mass spectrometer, and changes in the efficiency of the ionization and detection systems of the mass spectrometer.

2.7 Gold Calibration

Before carrying out quantitative measurements of nickel vaporization, a transmission calibration experiment was performed to determine the relative sensitivity factors for the four effusion holes of the quad-cell [15]. Gold was selected as the reference material, and contained in graphite crucibles in a graphite quad-cell (Fig. 1a), in accordance with accepted procedure for gold standard vapour pressure measurements [29], since gold does not react with graphite.

The second-law enthalpy of vaporization of gold was also determined for each compartment of the quad-cell. Since the largest circumferential temperature gradients in the present system were obtained with graphite quad-cells, comparison of the calculated ΔH°_{298} values with the accepted literature value would enable a check on the reliability of the system under "worst-case" conditions.

3. RESULTS

3.1 Container Interactions

3.1.1 Graphite Quad-Cells

Liquid nickel contained in graphite crucibles at about 1770K reacted with the graphite, and when cooled the bond was sufficiently strong that the solidified nickel could not be removed without breaking the crucible. Also, the surface of the nickel lost its shiny metallic appearance, and became dull grey in colour. Very little nickel vapour was found to have condensed on the cell walls.

A cross-sectional view of such a crucible is shown in Fig. 2a, where a reaction zone is visible in the underlying graphite. Figs. 2b and 2c of the same specimen under parallel illumination show more clearly the erosion of the crucible by the melt, the graphite precipitated from the melt, and graphite on the surface of the melt. Chemical analysis of the nickel residues was not considered feasible due to the difficulty of removing and analysing a very small amount of material from the crucible. Electron probe microanalysis could be carried out on a sectioned and polished sample, but the existing MRL facility is unable to quantitatively determine carbon composition. Comparison with pure nickel standards might enable an estimate of carbon composition by difference, but was not attempted.

Attempts were made to measure the lattice parameter of the f.c.c. nickel residue from melts in graphite crucibles, so that the carbon concentration could be determined from the relationship between lattice parameter and carbon content [30]. However, Debye-Scherrer X-ray powder diffraction patterns using Cu-Kα radiation produced very diffuse high angle f.c.c. reflections which could not be indexed.

3.1.2 Graphite Cells and Alumina Crucibles

Several experiments were conducted with a graphite quad-cell in which the walls of some cells were covered with a coating of alumina powder, deposited from a slurry in methanol and then dried at about 420K. The underside of the graphite lid was similarly coated so that no graphite was directly exposed within the cell. Nickel was placed directly in the cell or in alumina crucibles. A cell with exposed graphite walls and nickel in a

graphite crucible was used as a reference. At 1573K all the cells containing alumina displayed a position-dependent mass spectrum peak at $\frac{m}{e} = 28$, corresponding to CO emanating from the orifice. No such peak was observed from the alumina-free cell. Similarly, peaks corresponding to CO_2^+, AlO^+ and Al_2O^+ were identified only for the cells containing alumina. Furthermore, the CO evolution was sufficiently great that all background peaks were increased for the cells containing alumina, indicating that Knudsen conditions no longer prevailed and that no reliable thermodynamic data could be obtained from such cells. Cell residues showed signs of reaction, with a thin light blue coating on the nickel residues and the alumina crucibles, irrespective of whether the cell walls were alumina coated or left exposed. In addition, there was a thick grey reaction layer on the nickel shot placed directly in the alumina-coated cell (Fig. 3). A fine metallic lacework had grown beneath the alumina-coated lids of two cells (Fig. 4) and SEM examination revealed a dendritic structure (Fig. 5). Energy dispersive X-ray analysis (Fig. 5) showed the presence of nickel and aluminium, and area scans and spot analyses indicated that the aluminium was fairly uniformly distributed throughout the lacework, and was not the result of discrete particles of alumina adhering to the nickel. Overall, there was evidence of substantial metallic transport within each cell compartment at temperatures well below the melting point of nickel.

In contrast, there was no sign of metallic transport in the all-graphite cell, although the nickel shot had melted. Reference to the Ni-C phase diagram [17] shows that the nickel composition must be close to that of the eutectic composition at about 10 at.%C and 1591K, but the residue was not chemically analyzed.

3.1.3 Graphite Cells and Boron Nitride, Zirconia Crucibles

Boron nitride was found to be unsuitable as a container for nickel at temperatures above 1900K, both because the boron nitride adhered to the graphite, and because there was a significant amount of nitrogen decomposition product detected by the mass spectrometer, which led to erratic Ni^+ intensities and high background levels. A cross-section of the boron nitride crucible which was broken away from the graphite cell base is shown in Fig. 6. Some reaction with the nickel melt is evident in this cross-section.

Zirconia crucibles were also unsatisfactory as containers for nickel in graphite quad-cells, even though there was no visible reaction with the nickel (Fig. 7). Reaction between the zirconia and graphite occurred, however, because substantial CO was evolved at temperatures above 1800K, the crucibles turned grey indicating substoichiometric ZrO_{2-x}, and the crucibles often developed cracks which allowed leakage of the molten nickel. The reaction between the zirconia and graphite could be minimized by inserting a molybdenum foil between them, allowing some mass spectrometric measurements to be made.

3.1.4 Refractory Metal Quad-Cells and Ceramic Crucibles

Both alumina and zirconia were found to be suitable containers for molten nickel in molybdenum quad-cells, with no visible reaction with the nickel (Fig. 8) or with the molybdenum interior of the cell. However, the cell design shown in Fig. 1a was unsatisfactory since the equilibrium vapour pressure of nickel produces condensation of nickel throughout the cell, which subsequently reacts with the molybdenum, is transported by surface creep into and through the effusion orifice, which leads to the eventual blockage of the orifice.

The cell design shown in Fig. 1b was successful in overcoming the above problems. However, when held for extended periods at temperatures above 1800K, vaporization of the alumina occurred from the external surface surrounding the orifice, where the alumina was not covered by the molybdenum quad-cell. This resulted in a gradual shortening of the length of the effusion hole, and a consequent change in the transmission properties of the cell. There was no substantial improvement by replacing the molybdenum quad-cell with one made from tungsten.

When comparative tests were conducted using alumina and calcia-stabilized zirconia crucibles in adjacent compartments of a tungsten quad-cell, the zirconia crucibles were significantly more resistant to vaporization in the temperature range where alumina vaporized appreciably.

3.2 Gold Calibration

As described in Section 2.7, a transmission calibration experiment was performed using gold to determine the relative sensitivity factors for the four effusion holes of a graphite quad cell. The sensitivity factors were found to all fall within the range 1.00 ± 0.05, and this held for most of the quad-cells used in this study.

A second-law plot of $\ln(I^{+}_{Au} T)$ versus $\frac{1}{T}$ is shown in Fig. 9 for one of the four effusion holes, and the calculated ΔH_T and ΔH^{o}_{298} enthalpies of vaporization for all four effusion holes are shown in Table 2. The enthalpy functions of Hultgren et al. [6] were used. The close agreement between the four compartments, and with the recommended literature value [29], ΔH^{o}_{298} = 367.02 ± 0.88 kJ mol^{-1}, indicates that reliable second-law thermodynamic data can be obtained from the system, provided that appropriate temperature corrections are applied.

A further gold calibration was carried out during the course of the nickel vaporization experiments, to verify that the enthalpies of vaporization for nickel were free from substantial temperature errors. Attempts to carry out simultaneous measurements on nickel and gold in adjacent compartments of a graphite quad-cell were unsuccessful due to the vapour pressure of gold being about five times that of nickel in the temperature range 1800-2000K. This caused rapid depletion of the gold and condensation problems within the furnace. Therefore the nickel vaporization and calibration experiments were carried out sequentially, with minimal disturbance to the system when the gold

was added to the quad-cell. The second-law plot is shown in Fig. 10 and the enthalpy of vaporization is given in Table 2, in good agreement with the literature value.

3.3 Nickel Mass Spectrometry

3.3.1 Appearance Potentials

Electron energies usually are chosen to be only a few volts above the appearance potential (A.P.) of the ion in question (A.P. for Ni^+ is 7.633 eV [31]), to minimise possible fragmentation effects. In the present work, the ionization efficiency curve of $^{58}Ni^+$ for nickel in a graphite cell at 1973K was quite complex at electron energies between 9 eV and 20 eV (Fig. 11). A similar curve was obtained for nickel in an alumina cell at 1973K, indicating that the complex behaviour is probably not dictated by the interaction of nickel with its container. At ambient temperature, the $^{40}Ar^+$ ionization efficiency curve had the usual shape (Fig. 12) and yielded an appearance potential of 15.2 ± 0.5 eV, in good agreement with the literature ionization potential of 15.755 eV [31]. When the electron energy scale is corrected by 0.5 eV, the linearly extrapolated appearance potential for Ni^+ obtained from Fig. 11 is 7.3 ± 0.5 eV, in reasonable agreement with the literature value.

The cause of the complex ionization efficiency curves is at present unknown, and warrants further investigation. One possibility, that energetic ions were formed in the vicinity of the cell by electron bombardment of the effusing beam, was eliminated by appropriate experimentation. The nickel ion current monitored with the cell at 1973K did not change appreciably when the electron beam heating was switched off momentarily, indicating that there was little contribution of energetic ions to the measured ion current.

However, for the purpose of the present study, it was possible to avoid the complex region by using electron energies of ~35 eV, where the ion current is fairly insensitive to slight changes in electron energy. The measured $^{58}Ni^+$ signal may therefore contain some contribution from fragmentation of nickel vapour species other than Ni(g). A survey of the literature on gaseous positive nickel ions [31] indicates that NiO(g) and $Ni(CO)_4$ (g) are the only two likely sources of fragment ions, and could arise from the relatively high carbon and oxygen impurity levels of the nickel (Section 2.2).

The appearance potential of Ni^+ formed by fragmentation of $Ni(CO)_4$ (g) is 16.0 ± 0.3 eV which is attributed [32] to the probable process

$$Ni\ (CO)_4\ (g) \longrightarrow Ni^+ + 4\ CO\ (g) \qquad (10)$$

The appearance potential of Ni^+ formed by fragmentation of NiO (g) can be estimated from the relationship

$$AP(Ni^+) = IP(Ni^+) + D^\circ_0(NiO) \qquad (11)$$

where IP (Ni^+) is the ionization potential of nickel, 7.633 eV, and D°_0 (NiO) is the dissociation energy of NiO (g), 4.02 ± 0.04 eV, recalculated by Rutner and Haury [14] from the data of Grimley, Burns and Inghram [12]. The calculated appearance potential, 11.65 eV, corresponds closely with the onset of an increased Ni^+ ion current observed in the present ionization efficiency curve (Fig. 11). The Ni^+ from $Ni(CO)_4$ fragmentation would have an appearance potential which corresponds closely with the next onset of increased Ni^+ ion current. Further studies are necessary to determine whether these vapour species are actually present and in what concentration - no sign was observed in the present work of NiO^+ or $Ni(CO)_n^+$ ions. Winters and Kiser [32] have reported appearance potentials and abundance as a function of electron energy for all the singly-charged $Ni(CO)_n^+$ ions, with n varying from one to four. From thermodynamic considerations, it is expected that the partial pressure of NiO (g) and $Ni(CO)_4$ (g) above essentially pure Ni(c) should be very small at 2000K, and so should their corresponding fragmentation contributions to the observed Ni^+ ion current.

3.3.2 Nickel Vaporization

Second-law plots of $\ln(I^+_{Ni} T)$ versus $\frac{1}{T}$ are shown in Figs. 13-18 for Experiments 1-6, the details of which are given in Table 3. The second-law plots were analyzed by the method of least squares and the calculated enthalpies of vaporization are also presented in Table 3. The errors given for individual values of ΔH_T are 95% confidence limits, and the ΔH_T values are ascribed to the mid-point of the stated temperature range. The $\Delta H^\circ_{T\,298}$ values are calculated by equation 7.

In Experiments 1-3, nickel was contained in graphite crucibles inside graphite quad-cells. The same cell was used in Experiments 1 and 2 but the relative transmission factors were not calibrated. In Experiment 3 (Fig. 15) compartment B was pre-equilibrated by heating nickel in the graphite crucible for about three hours at 2050K with the lid on the compartment. At the same time, compartment C containing an empty crucible was thoroughly cleaned by leaving its lid off. In the subsequent mass spectrometry run, fresh nickel was added to compartment C, while B was left alone after ensuring that sufficient nickel remained in the crucible. The calculated enthalpy of vaporization of nickel from the pre-equilibrated compartment was significantly higher than that from the compartment containing fresh graphite and nickel. Furthermore, the ion current was approximately 2.5 times greater from the pre-equilibrated compartment B. A second gold calibration (using compartment A) was performed to verify the accuracy of the calculated enthalpies, as described in Section 3.2, and these results are shown in Fig. 10 and Table 2.

In Experiment 4 (Fig. 16), nickel was contained in an alumina crucible inside a molybdenum quad-cell, with the effusion orifice defined by the alumina crucible as in Fig. 1b. The calculated enthalpy is significantly higher than that for nickel in graphite, both new and pre-equilibrated. Only ion currents measured for liquid nickel have been included in the enthalpy

calculation, although the sensitivity was sufficient to measure strong ion currents below the nickel melting point, 1726K (Fig. 16). An increased slope in the second-law plot should be observed for the ion currents from solid nickel compared to liquid nickel, reflecting the enthalpy of melting of nickel, 17.47 kJ mol^{-1} [6]. Insufficient data points were recorded to verify ΔH_m, and the dashed line shown is an extrapolation of the liquid nickel data.

The results of Experiment 4 are confirmed in Experiment 5 (Fig. 17) in which nickel was contained in graphite and alumina crucibles respectively inside adjacent compartments of a molybdenum quad-cell. The alumina crucible arrangement was identical to that used in Experiment 4, while the compartment containing the graphite crucible had the effusion orifice defined by the molybdenum as in Fig. 1a. This introduced a possible complication in that the nickel vapour from the graphite crucible was contained within a molybdenum quad-cell, rather than a wholly graphite cell. The change in enthalpy observed for this compartment during the experiment will be discussed in Section 4. Since the relative transmission factors were not measured for the two effusion holes, it is not possible to accurately compare the magnitudes of the ion currents from each compartment. However, the observation that the ion current from the cell with the alumina crucible is three times greater than that from the compartment containing a graphite crucible is believed to be significant.

Although zirconia crucibles were unsatisfactory as long-term containers for nickel in graphite quad-cells (Section 3.1.3), useful information was obtained from short-term mass spectrometry anneals. Fig. 18 shows second-law plots (Experiment 6) for nickel vaporized from zirconia and graphite crucibles contained in a single graphite quad-cell. The quad-cell, of Fig. 1a design, had effusion orifices with identical transmission factors. The ion currents from the zirconia crucibles were approximately three times greater than those observed from the graphite crucible. The experimental arrangement within the cell was similar to that shown in Fig. 1a, except that a slot was cut in the extended crucible, opposite the effusion hole. In cell D the zirconia crucible was fitted with a zirconia lid, while that in cell B was not. The ion currents observed were marginally higher in cell D, reflecting the smaller area of graphite exposed to the nickel vapour. The calculated enthalpies of vaporization are shown in Table 3, and are significantly greater for the zirconia crucibles compared to the graphite crucible. In subsequent anneals of this system, the ion currents from cell C gradually increased and became closer to those of cells B and D, which remained essentially constant at any particular temperature. This confirms the gradual equilibration of nickel and graphite that was observed in Experiment 3. Insufficient data was collected in these subsequent anneals to verify whether the enthalpy of vaporization from cell C increased in accord with the ion current.

4. DISCUSSION

4.1 Container Interactions and Vaporization Thermodynamics

4.1.1 Graphite Crucibles and Quad-Cells

It is clear from the metallographic evidence that significant interaction occurs between molten nickel and graphite crucibles. This has a pronounced effect on the nickel vapour pressure and enthalpy of vaporization. The mean ΔH^{o}_{298} calculated from Experiments 1-3 for nickel in fresh graphite crucibles and quad-cells is 366 ± 6 kJ mol^{-1}, significantly lower than the literature average value of 428.3 ± 4 kJ mol^{-1}. Pre-equilibration of the graphite and nickel at a much higher temperature in an attempt to form a kinetically stable reaction layer was partially successful, in that the measured ΔH^{o}_{298} falls midway between the fresh graphite value and the literature value.

Although chemical analysis of the nickel residues was not carried out, estimates of the carbon concentration in liquid nickel may be made from the relationship reported by Shunk [17]

$$\log N_C = \frac{-895.7}{T(K)} - 0.462 \qquad (12)$$

which is valid for the temperature range 1623-2023K, where N_C is the atom fraction of carbon. The calculated carbon composition for the average temperature of each mass spectrometry run is shown in Table 4. There is insufficient range in the calculated compositions to establish any relationship between carbon composition and nickel enthalpy of vaporization. The initially high value of ΔH_T observed in Experiment 5 is subject to large errors since it is only based on three data points. Furthermore, there is the possibility of initial equilibration of the nickel vapour with the molybdenum quad-cell used in this experiment. However the subsequent ΔH_T is not significantly different from that obtained from graphite quad-cells, and it is believed that the interaction with graphite dominates the nickel enthalpy of vaporization.

The evidence from Experiment 3 for the establishment of a partially stable pre-equilibrated layer indicates that care must be taken in assigning the calculated carbon composition to the average temperature of each run, on the assumption of the establishment of rapid equilibrium between the graphite crucible and the melt. No obvious relationship exists between nickel enthalpy of vaporization and carbon composition calculated from the maximum temperature reached in each run.

4.1.2 Alumina and Zirconia Crucibles and Cells

Alumina crucibles were shown to be incompatible with graphite quad-cells, through reduction of the alumina and evolution of CO. The exact nature

of the reaction was not characterized, but probably follows reaction (1). Rinehart and Behrens [33] have shown that Al_4C_3 vaporizes incongruently in the temperature range 1300-1600K to give Al(g) and graphite as reaction products. The equilibrium vapour pressure of Al(g) at 1800K extrapolated from their data is 26 Pa.

The observation of reaction products in the cell residues when nickel was vaporized from Al_2O_3/graphite systems further highlights the incompatiblility. There was significant metallic transport throughout the cell, even though the nickel shot had not melted (anneal temperature was 1573K). Such transport could occur if the CO pressure was sufficiently high to enable volatilization of nickel as $Ni(CO)_4(g)$, although this species was not observed in the mass spectrometric analysis. The observation of aluminium in the dendritic nickel lacework provides evidence for the presence of Al(g) in the vapour, from reduction of the alumina by the graphite, as discussed above.

The metallographic evidence indicates that there is no interaction between molten nickel and alumina or zirconia crucibles. With appropriate quad-cell design, it has been shown (Table 3) that the calculated enthalpy of vaporization from alumina cells is in excellent agreement with the literature value. However, the vaporization of alumina from the vicinity of the effusion orifice, when held for extended periods at high temperature, does provide a limitation to accurate vapour pressure and hence activity measurements, due to the changing transmission factor for the orifice. The available evidence indicates that calcia stabilized zirconia crucibles will not show this limitation. A detailed study of the vaporization of nickel from zirconia crucibles, utilising both the second-and third-law methods, has not yet been possible. It awaits the availability of crucibles of the required geometry and density.

4.2 Errors in Enthalpies of Vaporization

The errors given in Tables 2 and 3 for the individual values of ΔH_T are 95% confidence limits, calculated from the slope of the $\ln(I_i^+T)$ versus 1/T least-squares plot. This gives a measure of the uncertainties caused by random errors. The errors attributed to the mean values are the standard deviations. Johnston and Burley [16] have discussed the role of temperature measurement as the major source of systematic errors, and the effect of a uniform temperature uncertainty across the range of temperature measurement. It can be shown that the percentage error in the calculated second-law enthalpy is approximately twice the percentage error in the true temperature, and about equal to the differential error in temperature divided by the temperature interval (x100) [34]. The differential temperature error is the difference between the absolute temperature errors at either end of the temperature range under study, and is a more important source of error than a uniform absolute error across the temperature range. Thus a uniform 10K error in T over the temperature interval 1900 to 2100K produces an error in ΔH_T of about 1%, whereas a differential error of 10K over that 200K interval causes an error of approximately 5%. Although this is of the same magnitude as the random errors (at the 95% confidence level) in Tables 2 and 3, the latter errors can be reduced by measuring a greater number of data

points in individual determinations of ΔH_T. Indeed the standard deviation of the mean of the combined measurements from four compartments is significantly lower. The above considerations therefore highlight the need to minimise differential temperature errors in accurate second-law measurements. The excellent agreement between the experimentally-measured and literature values for the enthalpy of vaporization of gold indicates that there were no large differential temperature errors present in this work.

4.3 Activity Measurements in Multicomponent Nickel Alloys

As was discussed in the Introduction, the present study was undertaken as a preliminary to the determination of both nickel and aluminium activities across the complete compositional range of the nickel-aluminium system. In the previous study [1] of the high nickel compositions ($x_{Ni} > 0.54$) it was reported that materials problems prevented the determination of aluminium activities. In the light of the present results, it is necessary to consider whether the reported nickel activities may also be considerably in error.

The thermodynamic activity a_{Ni} of nickel in a binary alloy is given by

$$a_{Ni} = \frac{P_{Ni}}{P^{o}_{Ni}} \qquad (11)$$

where P_{Ni} and P^{o}_{Ni} are the vapour pressures of nickel in equilibrium with the alloy and pure nickel, respectively. When pure nickel is in one compartment of the quad-cell and the alloy in another, and when the effusion holes of both compartments have identical transmission factors, then the nickel activity is given simply by the ratio of the ion currents

$$a_{Ni} = \frac{I_{Ni}}{I^{o}_{Ni}} \qquad (12)$$

where I_{Ni} and I^{o}_{Ni} are the mass-spectrometric ion currents for the alloy and pure nickel, respectively [15]. The ion current for nickel vaporized from a zirconia crucible (Experiment 6) was approximately three times that observed for nickel vaporized from a graphite crucible, both crucibles being contained in identical compartments of a graphite quad-cell. The activity of 'pure' nickel contained in the graphite crucible, therefore, was approximately one-third that of 'pure' nickel contained in the adjacent zirconia crucible. Indeed, it is likely that the ion current for nickel vaporized from the zirconia crucible was somewhat reduced due to the interaction of the vapour with the exposed internal graphite walls of the quad-cell. Therefore the true nickel activity of nickel saturated with graphite would be somewhat less than 0.3 at this temperature (~1890K).

The same method was used to determine nickel activities in nickel-aluminium alloys in graphite quad-cells [1]. The activities so determined

were in reality pseudo-activities, in that both the pure nickel and the nickel in the alloy underwent reaction with the graphite. The actual value of the pseudo-activity may correspond to that of the alloy in a non-reactive system, provided that only one component of the alloy (either nickel or aluminium) reacts with the crucible. However, where both components of the alloy react with the crucible, as is indicated in the case of nickel-aluminium alloys in graphite [1], the pseudo-activity for nickel then depends on the complex interactions between nickel, aluminium and carbon, across the composition range of the alloy.

The thermodynamic properties of the ternary nickel-aluminium-carbon system are likely to be quite different from that of the binary nickel-aluminium system. The phase boundaries have been determined at 1000°C [35]. No ternary Ni_3AlC_x phase was found, but γ'-Ni_3Al exhibits a solubility for carbon of up to 7-8 at.%. The phase β-NiAl was also found to dissolve carbon to about 3 at.%, but no solubility was detected in the phases Ni_2Al_3 and $NiAl_3$. A study [36] of the effect of carbon on ordering of γ'-Ni_3Al in rapidly solidified Ni_3Al-C alloys verifies that only an ordered Ni_3AlC_x ($x = 0 \sim 0.34$) single phase is formed.

The nickel activities reported in [1] refer to the ternary Ni-Al-C system, and, until they can be reproduced using a non-reactive crucible/quad cell system, their relevance to the binary Ni-Al system is somewhat uncertain. In such a non-reactive system, aluminium activities should then be simultaneously calculable. The nickel and aluminium activities should be self-consistent using the Gibbs-Duhem method of calculating the activity of one component from that of the other. Such consistency would be evidence of the absence of spurious container interactions.

The results from the present work indicate that stabilized zirconia crucibles contained in molybdenum or tungsten quad-cells, with the zirconia defining the effusion orifice, are likely to be suitable containers for nickel. Preliminary studies also indicate that such a system should be stable to liquid aluminium, and hence suitable for the thermodynamic study of the nickel-aluminium system over the complete range of compositions.

The above quad-cell/crucible combination should also be suitable to use in the recently commenced study of the nickel-aluminium-platinum system. This ternary system is of great interest since it constitutes the second-generation aluminide protective coating that has been applied with considerable success to the first-stage turbine blades in an Australian military gas turbine engine [37]. The platinum addition is extremely efficacious in reducing the degradation of the coating by high temperature corrosion [37]. Because little is known of the thermodynamic properties of this important system, the quad-cell mass spectrometry technique is being used to determine the individual component activities and hence the thermodynamic parameters of the Ni-Al-Pt system.

5. CONCLUSIONS

In this Report significant interactions have been shown to occur between nickel and various refractory containers commonly used in high-temperature Knudsen cell vaporization systems. In particular, graphite was shown to be an unsuitable container, considerably reducing the nickel activity and enthalpy of vaporization. Recrystallized alumina and stabilized zirconia refractories were stable to molten nickel, enabling the determination of valid thermodynamic data. Recommendations have been made for a suitable crucible/quad-cell system for the study of the thermodynamic properties of nickel-aluminium and nickel-aluminium-platinum alloys.

6. ACKNOWLEDGEMENT

The author is grateful to Mr F.A. Griffo for carrying out the polished section optical micrographs of the crucibles, and for verifying the ionization efficiency curve for nickel vaporized from an alumina cell.

7. REFERENCES

1. Johnston, G.R. and Palmer, L.D (1980). "Quad-cell mass spectrometry: thermodynamic properties of liquid aluminium-nickel alloys". *High Temp. - High Press.*, 12, 261-266.

2. Ward, J.W. and Mulford, R.N.R. (1967). "Study of some of the parameters affecting Knudsen effusion. I. Experimental tests of the validity of the cosine law as a function of cell and sample geometries and materials". *J. Chem. Phys.*, 47, 1710-1717.

3. Chatillon, C., Allibert, M., and Pattoret, A. (1979). "Thermodynamic and physico-chemical behaviour of the interactions between Knudsen-effusion-cells and the systems under investigation: analysis by high temperature mass spectrometry". *NBS, Special Publication, 561: Proceedings of the 10th materials research symposium on characterization of high temperature vapors and gases, NBS Gaithersburg, Maryland, Sept. 18-22, 1978*, 181-210.

4. Clark, N.J. and Mart, P.L. (1981). "Tungsten bronze-container interactions at high temperatures". *Mat. Res. Bull.*, 16, 127-135.

5. Mart, P.L. and Clark, N.J. (1982). "Vaporization of tungsten bronzes: cubic lithium bronzes". *High Temp. Sci.*, 15, 1-16.

6. Hultgren, R., Desai, P.D., Hawkins, D.T., Gleiser, M., Kelley, K.K. and Wagman, D.D. (1973). *"Selected values of the thermodynamic properties of the elements"*, Metals Park, Ohio, ASM, 350-357.

7. Nesmeyanov, An. N. (1963). *"Vapor pressure of the elements"*, (Transl. by Carasso, J.I.), Infosearch Limited, London, 390-397.

8. Nesmeyanov, An. N. and Man D.D. (1960). *Russian Metallurgy and Mining*, 1, 75-84.

9. Kovtun, G.P., Kruglykh, A.A. and Pavlov, V.S. (1962). "Vapour pressure and the evaporation coefficient of nickel". *Ukrain. Fiz. Zh.*, 7, (4), 436-438.

10. Alcock, C.B. and Kubik, A. (1968). "Thermodynamic behaviour of liquid iron-cobalt and nickel-platinum alloys". *Trans. Inst. Min. Met.*, 77, C220-C224.

11. Lindscheid, H. and Lange, K.W. (1970). "Vapour pressure measurements of binary alloys containing two volatile components." *Z. Metallkde*, 61, 193-200.

12. Grimley, R.T., Burns, R.P. and Inghram, M.G. (1961). "Thermodynamics of the vaporization of nickel oxide". *J. Chem. Phys.*, 35, (2), 551-554.

13. Vrestal, J. and Kucera, J. (1971). "Determination of nickel vapor pressures by an effusion method using nickel-63". *Jad. Energ.*, 17, (5), 158-160.

[illegible]. "The vapor pressure and [illegible] vaporization of nickel". *Report AFML-TR-[illegible]*, Air Force Materials Laboratory, Wright-Patterson Air Force Base, [illegible]. (Available NTIS as AD-[illegible] 332).

[illegible]. Johnston, G.R. (1977). "High temperature vaporization studies [illegible] multi-cell mass spectrometry". In *Dynamic mass spectrometry*, D. and Williams, J.E. eds.), Vol. 5, London, Heyden, 206-[illegible].

[illegible]. Johnston, G.R. and Burley, N.A. (1977). "Quad-cell mass spectrometer vaporization studies up to 2300K using a rotatable, multiple Knudsen cell ('quad-cell')". In *Proceedings of the seventh symposium on thermophysical properties, NBS, Gaithersburg, Maryland, May 30-31, 1977* (Cezairliyan, A. ed.), N.Y., American Society of Mechanical Engineers, 222-230.

[illegible]. Hansen, M. (1958). *Constitution of binary alloys*, McGraw-Hill, New York, and supplements:
Elliott, R.P. (1965), First supplement.
Shunk, F.A. (1969), Second supplement.

[illegible]. Moffatt, W.G. (1978). *The handbook of binary phase diagrams*, General Electric, New York.

[illegible]. Bradley, D.J., Leitnaker, J.M. and Horne, F.H. (1982). "Thermodynamics of carbon in Ni-C alloys from 900 to 1215°C". *High Temp. Sci.*, [illegible] 187-198.

[illegible]. Elliott, J.F. and Gleiser, M. (1960). *Thermochemistry for steelmaking*, Vol. I, Addison-Wesley, London, 214-215.

[illegible]. Jansson, S.A. (1971). "Thermochemistry of liquid metal-gas [illegible] reactions in vacuum". *J. Vac. Sci. Tech.*, 7, (6), 85-[illegible].

[illegible]. Foster, L.M., Long, G. and Hunter, M.S. (1956). "Reactions between aluminum oxide and carbon. The Al_2O_3-Al_4C_3 phase diagram". *J. Amer. Ceram. Soc.*, 39, (1), 1-11.

[illegible]. Kubaschewski, O. and Alcock, C.B. (1979). *Metallurgical thermochemistry*, 5th ed., Pergamon Press, Oxford, 384.

[illegible]. Stull, D.R. and Prophet, H. (1971). *JANAF thermochemical tables*, 2nd ed., NSRDS-NBS 37.

[illegible]. Yurchenko, O.S. (1971). "Iron and nickel stability during [illegible] contact with refractory compounds", *Porosh. Met.*, 11 (1), 4[illegible].

26. Bockris, J. O'M., White, J.L. and Mackenzie, J.D. (1959). *Physicochemical measurements at high temperatures*, Butterworths, London, 25-26.

27. Yudin, B.F. and Markholiya, T.P. (1967). "Reaction thermodynamics ZrO_2, MgO, and CaO with refractory metals". *All-Union Inst. of Refractories*, (USSR), 440-446.

28. Markholiya, P.P., Yudin, B.I. and Vol'kin, N.I. (1965). "Interaction of high-melting metals with aluminium oxide and silicon dioxide". *In Fiz. Tugkoplavk. Metal., Tr. Vses. Soveshch., 2nd, Leningrad*, 203-208 (Publ. 1967).

29. Paule, R.C. and Mandel, J. (1970). "Analysis of interlaboratory measurements on the vapor pressure of gold". NBS Spec. Publ. 260-19.

30. Ruhl, R.C. and Cohen, M. (1967). "Metastable extensions of carbon solubility in nickel and cobalt". *Scripta Metallurgica* 1, 73-74.

31. Franklin, J.L., Dillard, J.G., Rosenstock, H.M., Herron, J.T., Draxl, K. and Field, F.H. (1969). "Ionization potentials, appearance potentials, and heats of formation of gaseous positive ions". NSRDS-NBS 26.

32. Winters, R.E. and Kiser, R.W. (1964). "A mass spectrometric investigation of nickel tetracarbonyl and iron pentacarbonyl". *Inorg. Chem.*, 3, (5), 699-702.

33. Rinehart, G.H. and Behrens, R.G. (1980). "Vaporization thermodynamics of aluminium carbide". *J. Chem. Thermodyn.*, 12, 205-215.

34. Ackermann, R.J. and Thorn, R.J. (1961). "Vaporization of Oxides". In *Progress in ceramic science*, Vol. I (Burke, J.E. ed.), Pergamon, Oxford, 42.

35. Schuster, J.C. and Nowotny, H. (1982). "The ternary system nickel-aluminium-carbon". *Monatsh. Chem.*, 113, 163-170.

36. Han, K.H. and Choo, W.K. (1983). "Carbon effect on ordering of γ'-Ni_3Al in rapidly solidified Ni_3Al-C alloys". *Scripta Metallurgica*, 17, 281-284.

37. Johnston, G.R. and Richards, P.G. (1981). "High-temperature corrosion in military gas turbines: an initial metallographic comparison of the durability of two protective coatings (PWA 73 and RT22) for first-stage turbine blades in TF30-P-3 engines (U)." *Report MRL-R-820*, Materials Research Laboratories, Melbourne, Victoria. Restricted report.

T A B L E 2

Enthalpy of Vaporization of Gold from Graphite Quad -Cells

Compartment	T Range (K)	ΔH_T * (kJ mol^{-1})	ΔH°_{298} (kJ mol^{-1})
Calibration No. 1			
A	1688 -1933	344.8 ± 24.4	370
B		343.4 ± 23.9	368
C		345.5 ± 24.5	370
D		346.2 ± 28.6	371
		mean 345.0 ± 1.2	370
Calibration No. 2			
A	1667 - 1890	345.4 ± 23.9	370

* 95% confidence limits on individual values, ± standard deviation on mean.

TABLE 4

Enthalpy of Vaporization of Nickel from Various Crucibles and Quad-Cells

Expt.	Compartment (crucible)	T range (K)	ΔH_T * (kJ mol^{-1})	ΔH^o_{298} (kJ mol^{-1})
1.	Graphite quad-cell, graphite crucibles			
	A	1790 - 2015	333.0 ± 18.7	367
	B		335.0 ± 15.5	369
	C		337.1 ± 24.4	371
	D		339.3 ± 24.0	373
		mean	336.1 ± 2.7	370
2.	Graphite quad-cell, graphite crucibles			
	A	1827-1972	325.5 ± 7.6	359
	B		325.3 ± 15.6	359
	C		329.6 ± 15.6	363
	D		339.4 ± 14.7	373
		mean	330.0 ± 6.6	364
3.	Graphite quad-cell, graphite crucibles			
	B (pre-equilibrated)	1753 - 2020	351.5 ± 9.6	385
	C (new)		327.6 ± 20.4	361
4.	Molybdenum quad-cell, alumina crucible			
	A	1734 - 1895	404.2 ± 17.4	436
5.	Molybdenum quad-cell, alumina and graphite crucibles			
	B (alumina)	1736 - 1918	393.1 ± 13.3	425
	C (graphite)	1721 - 1825	(400 ± 59) (pts. 1-3)	431
		1728 - 1918	332.3 ± 13.0 (pts. 4-10)	364
6.	Graphite quad-cell, zirconia and graphite crucibles			
	C (graphite)	1794 - 1995	331.8 ± 20.5	365
	B (zirconia)		356.1 ± 29.9	390
	D (zirconia + lid)		355.5 ± 38.5	389

* 95% confidence limits on individual values, ± standard deviation on means.

TABLE 4

Calculated Carbon Composition of Nickel and Enthalpy of Vaporization of Nickel

Expt.	T average (K)	N_C average	ΔH_T * (kJ mol^{-1})
Graphite quad-cells, graphite crucibles (new)			
1.	1903	0.117	mean 336.1 ± 2.7
2.	1900	0.117	mean 330.0 ± 6.6
3.	1887	0.116	327.6 ± 20.4
6.	1895	0.116	331.9 ± 20.5
Molybdenum quad-cell, graphite crucible			
5.	1773 (pts. 1-3)	0.108	(400 ± 59)
	1823 (pts. 4-10)	0.111	332.3 ± 13.0

* 95% confidence limits on individual values, ± standard deviation on means.

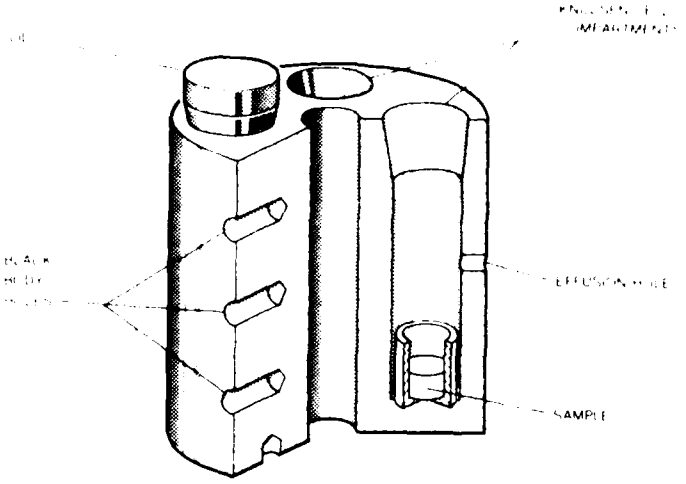

Fig. 1a. Quad-cell with crucible containing sample (after Johnston [15]).

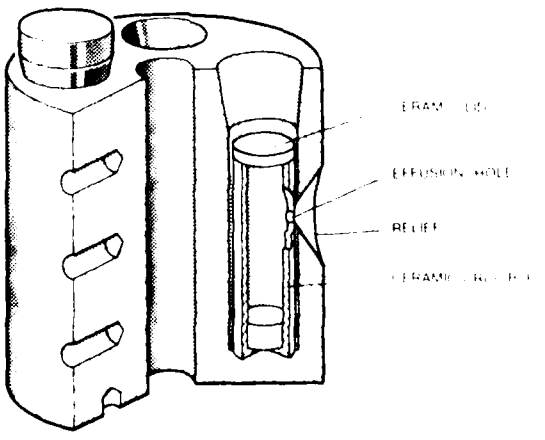

Fig. 1b. Quad-cell with ceramic liner as Knudsen cell.

(a) Magnification 1X

(b) 15 X

(c) 90 X

FIG. 2. Optical micrograph [illegible] in graphite crucible, annealed in graphite [illegible].

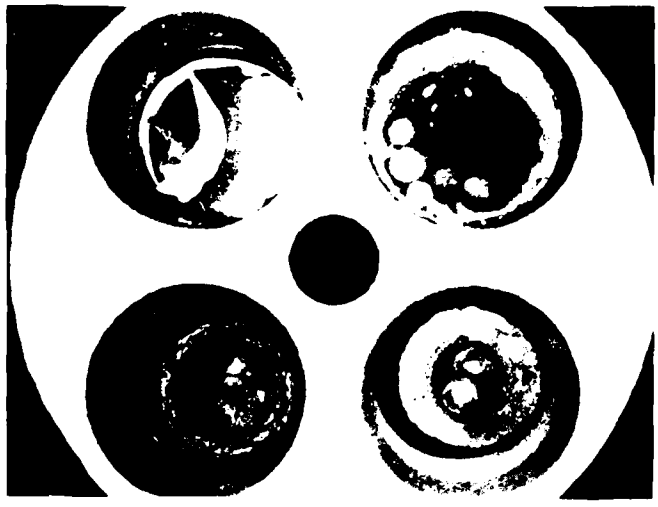

FIG. 3. Nickel in graphite quad-cell annealed at 1573K (magnification ~ 4 X).

Top L. - Al_2O_3 coating and crucible, metallic lacework, blue deposit.

Top R. - Al_2O_3 coating, metallic deposit, reaction layer on Ni.

Bot L. - Graphite walls and crucible, Ni melted.

Bot R. - Graphite walls, Al_2O_3 crucible, blue deposit throughout cell.

FIG. 4. Metallic lacework from beneath lid (Top L. cell, Fig. 3) (magnification 9 X).

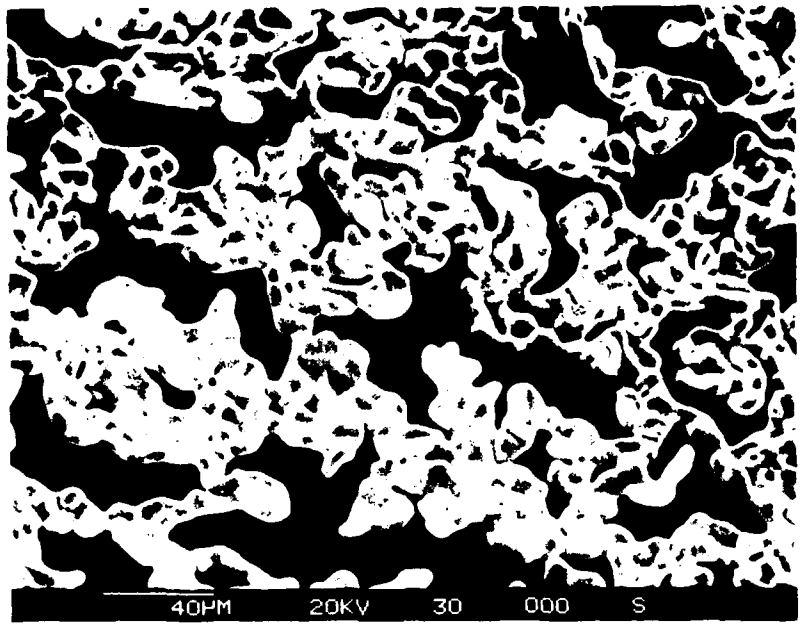

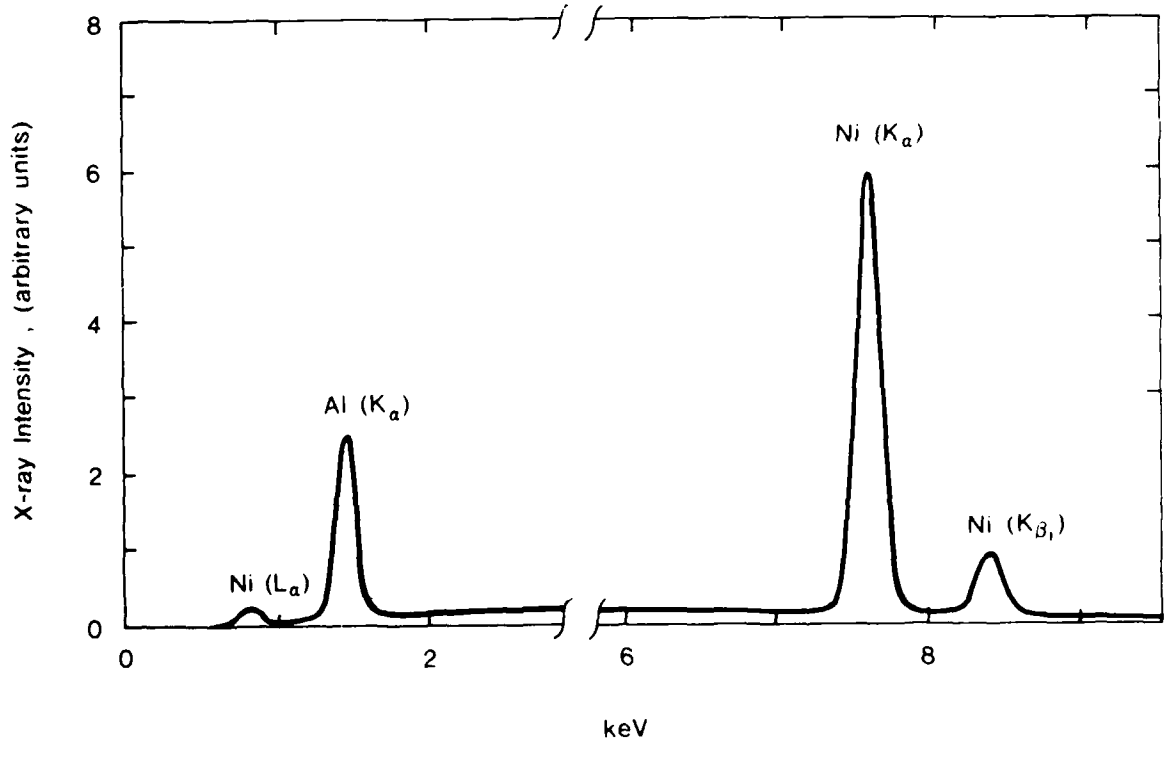

FIG. 5. Scanning electron micrograph and Energy Dispersive X-Ray analysis (same area) of metallic lacework in Fig. 4.

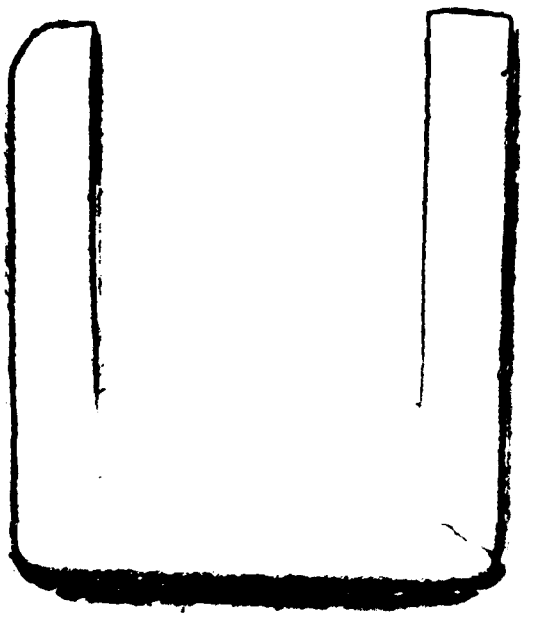

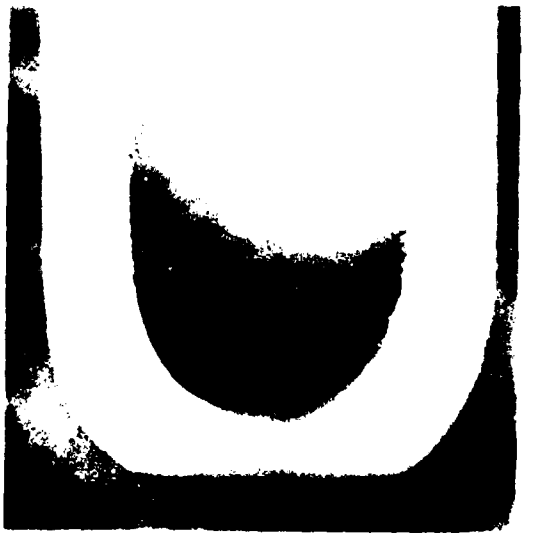

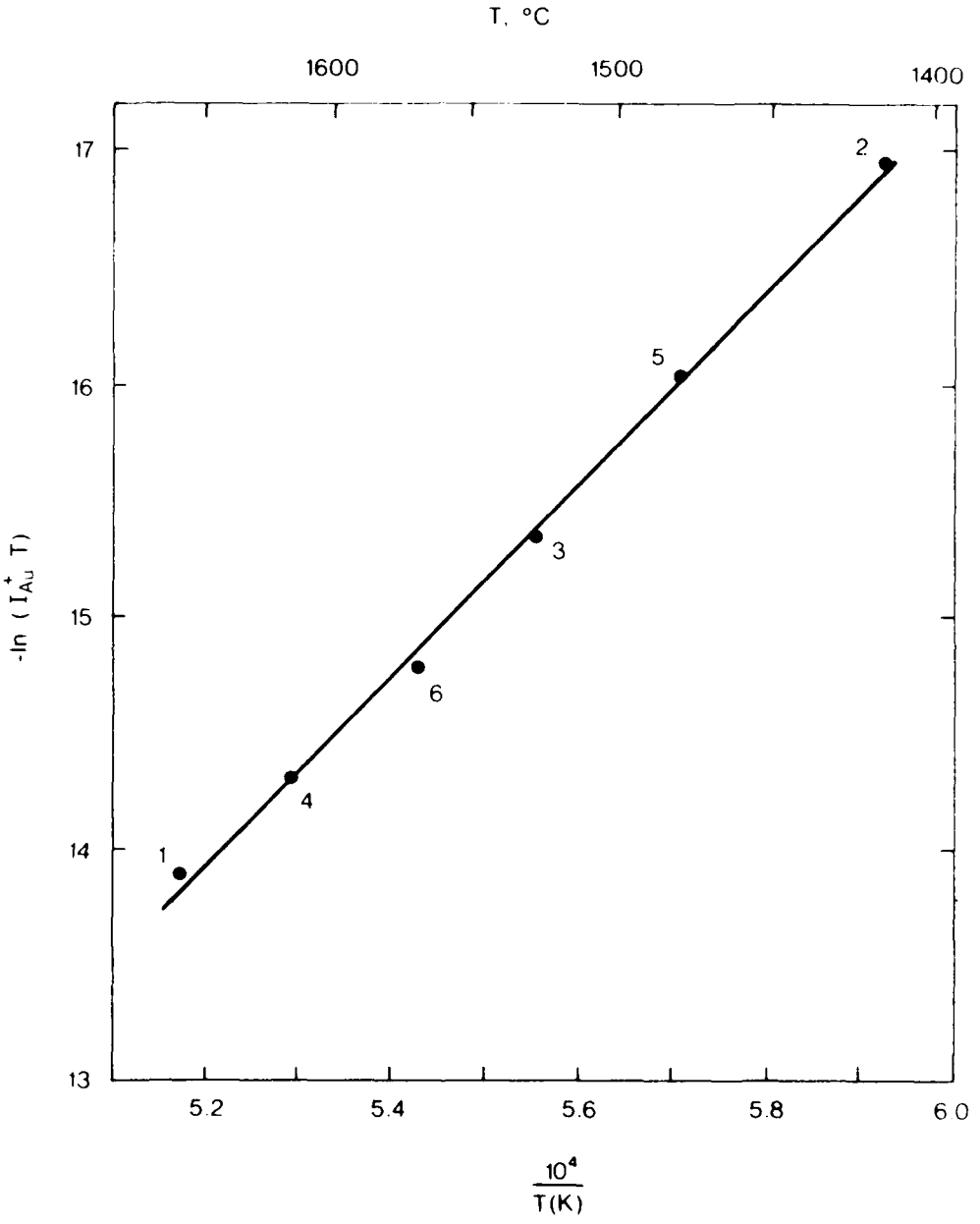

FIG. 9. Gold calibration No. 1. Second-law plot of ln (I_{Au}^{+} T) versus $\frac{1}{T}$ for gold vaporized from graphite quad-cell.

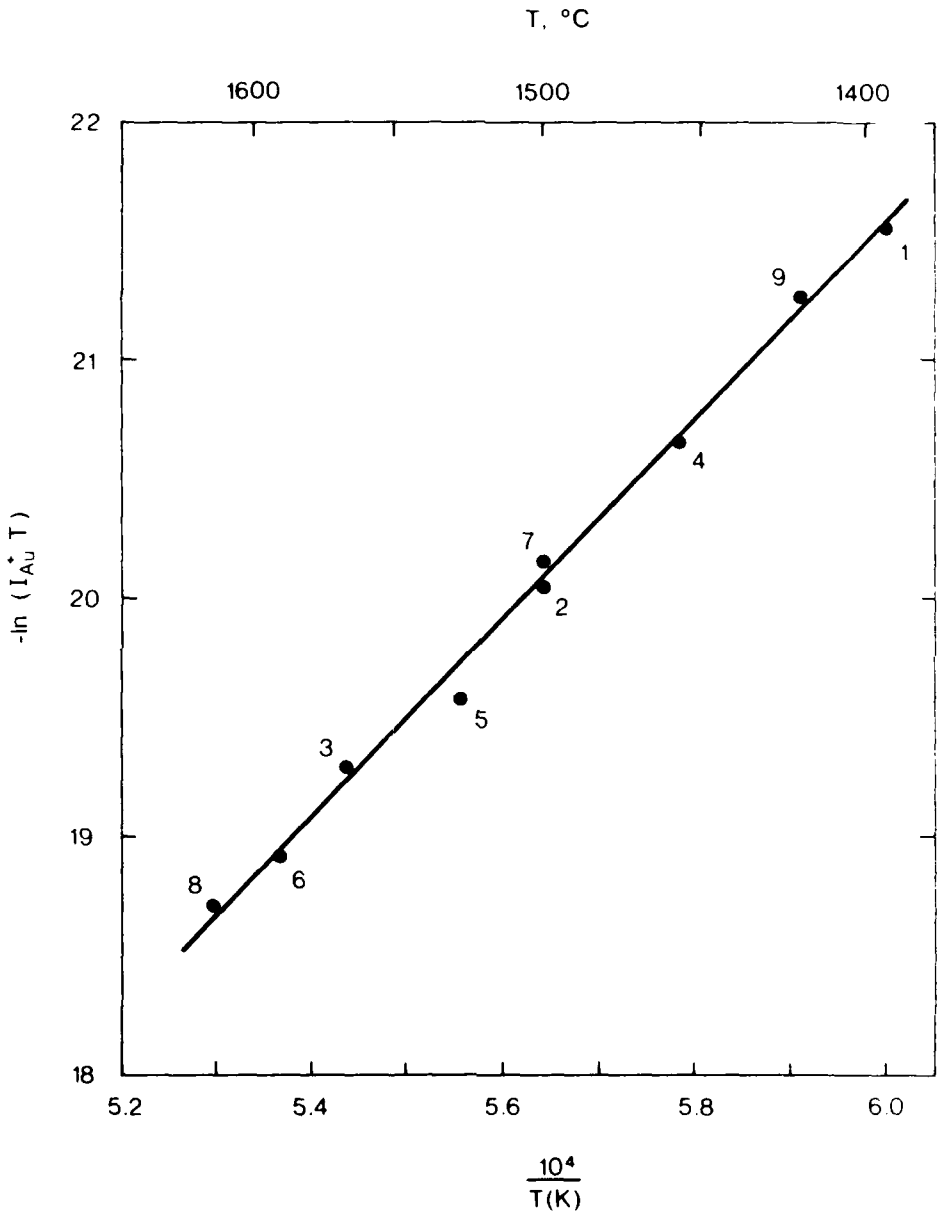

FIG. 10. Gold calibration No. 2. Second-law plot of ln (I_{Au}^{+} T) versus $\frac{1}{T}$ for gold vaporized from graphite quad-cell.

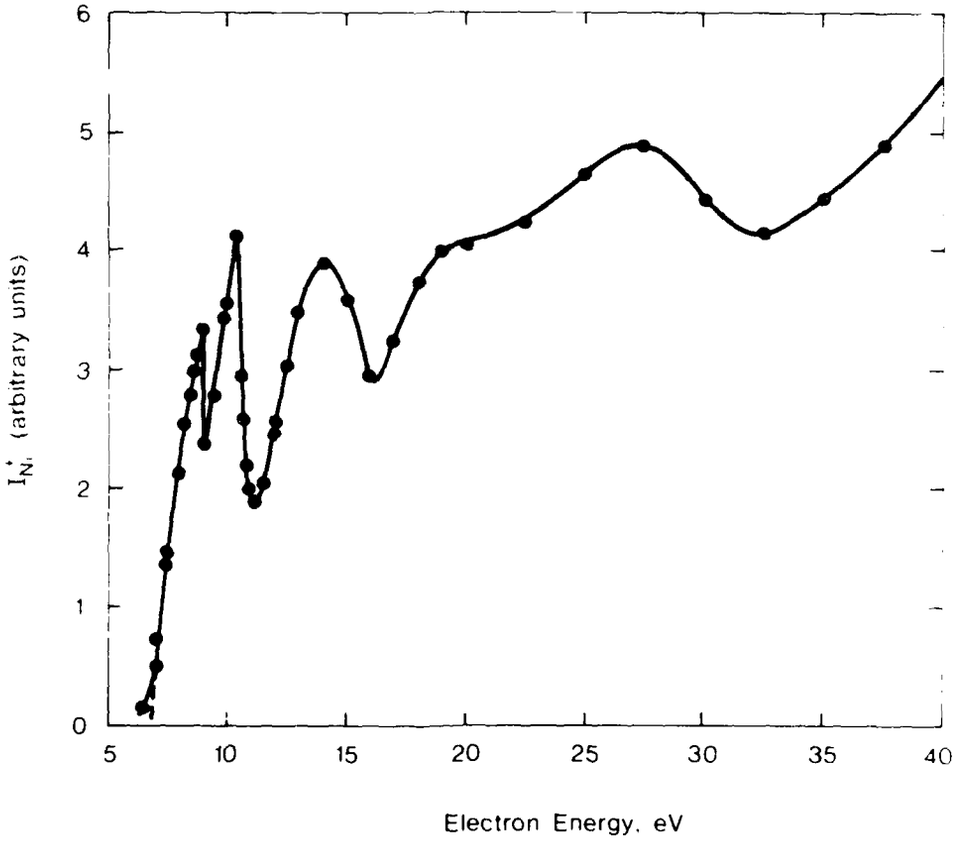

FIG. 11. Ionization efficiency curve for nickel vaporized from graphite quad-cell at 1973K.

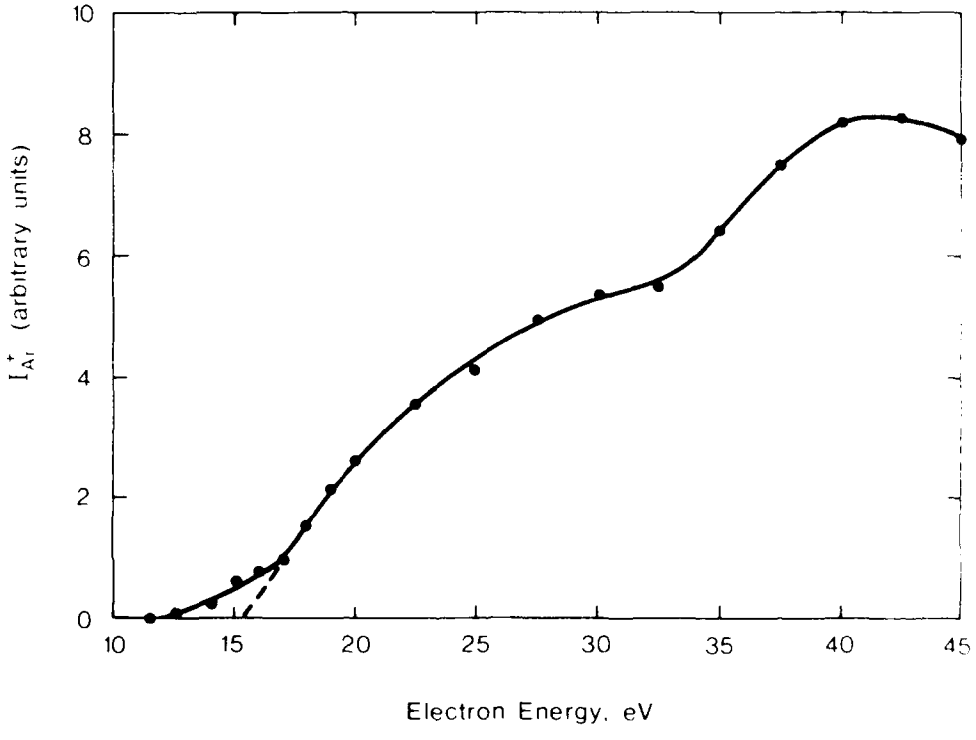

FIG. 11. Ionization efficiency curve for argon at ambient temperature (298K).

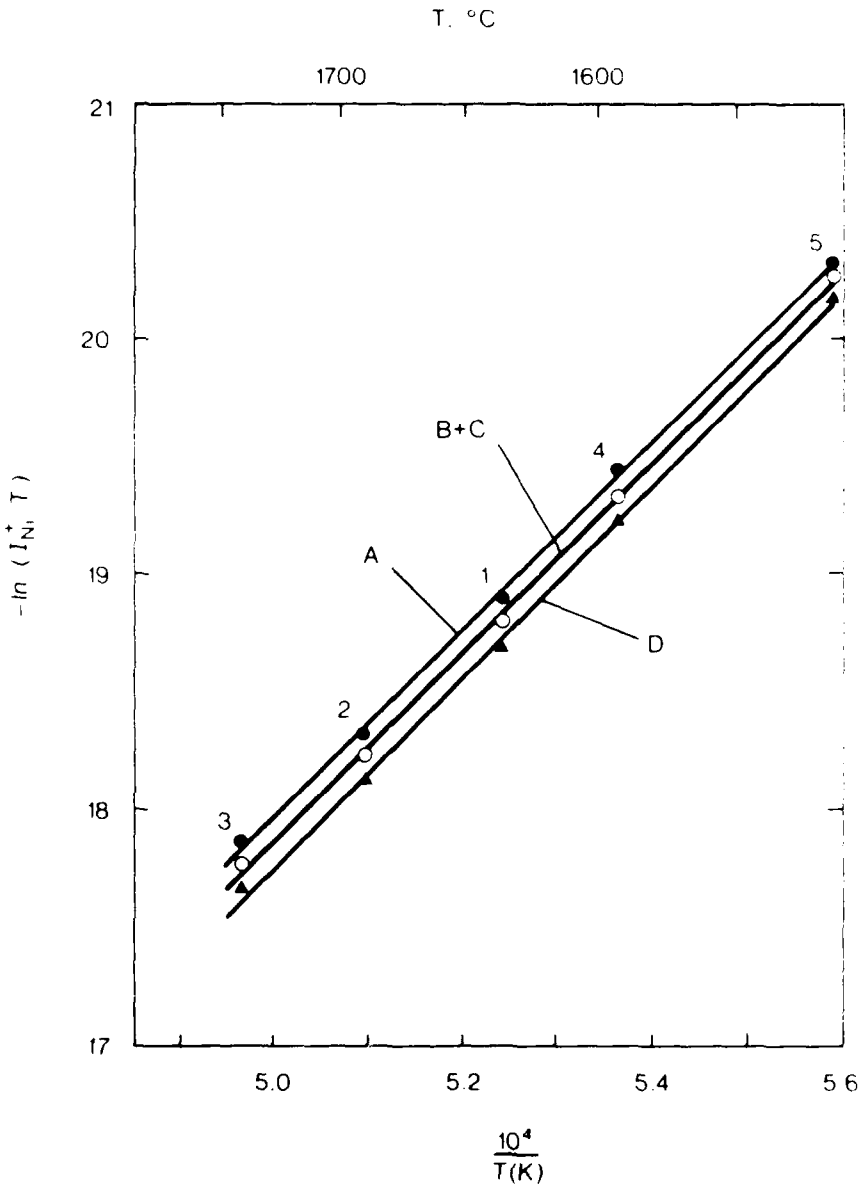

FIG. 13. Second-law plots for nickel vaporized from graphite crucibles in a graphite quad-cell. Ionizing electron energy 50 eV.

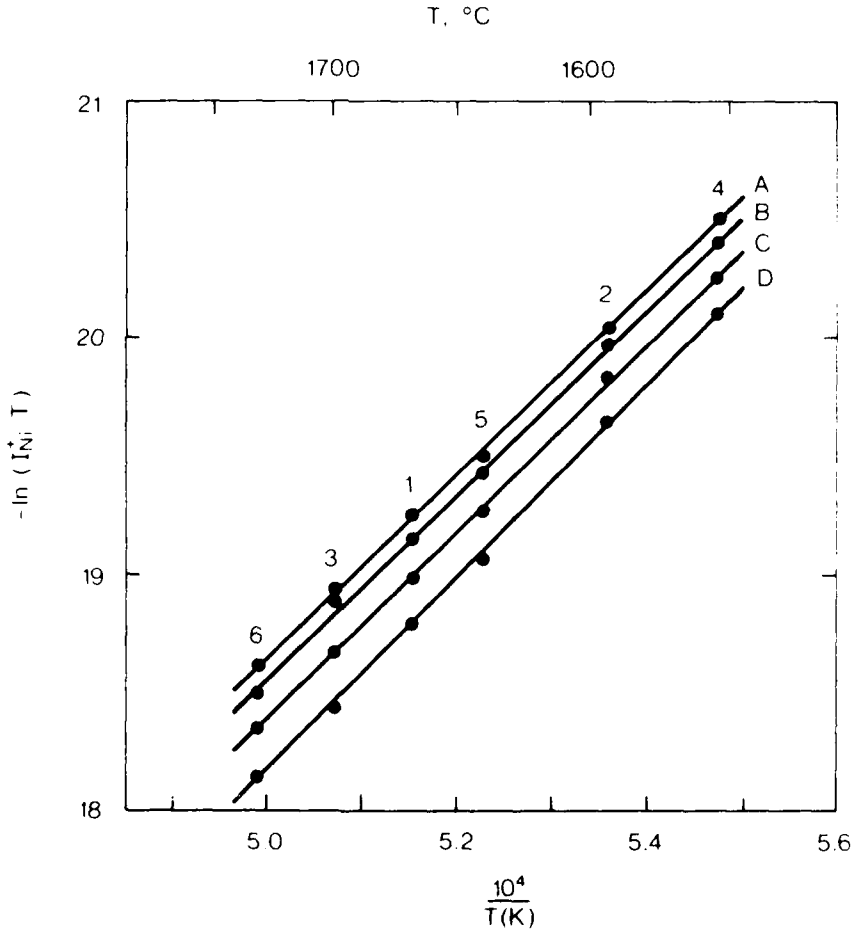

FIG. 14. Second-law plots for nickel vaporized from graphite crucibles in a graphite quad-cell. Ionizing electron energy 40 eV.

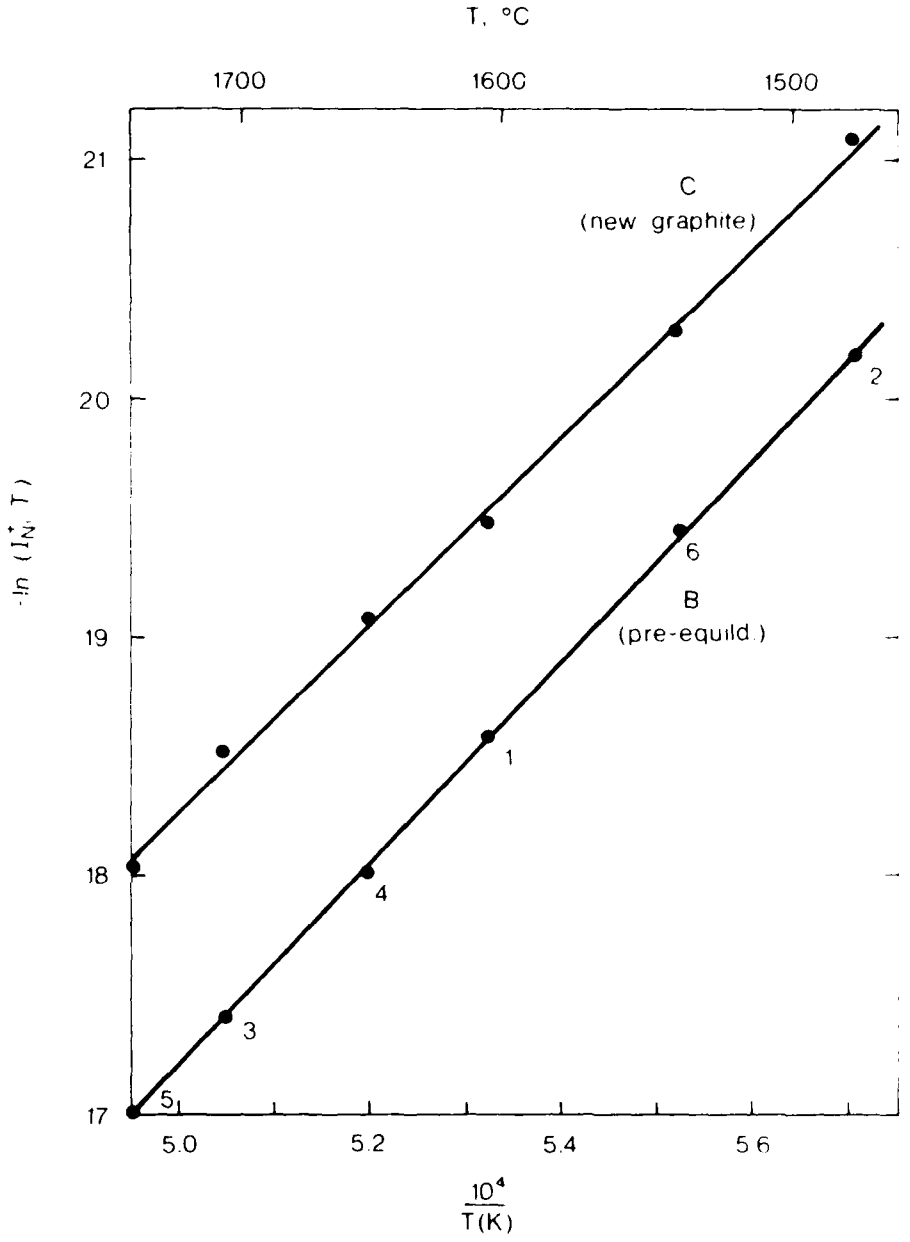

FIG. 15. Second-law plots for nickel vaporized from graphite crucibles (B pre-equilibrated, C new) in a graphite quad-cell. Ionizing electron energy 35 eV.

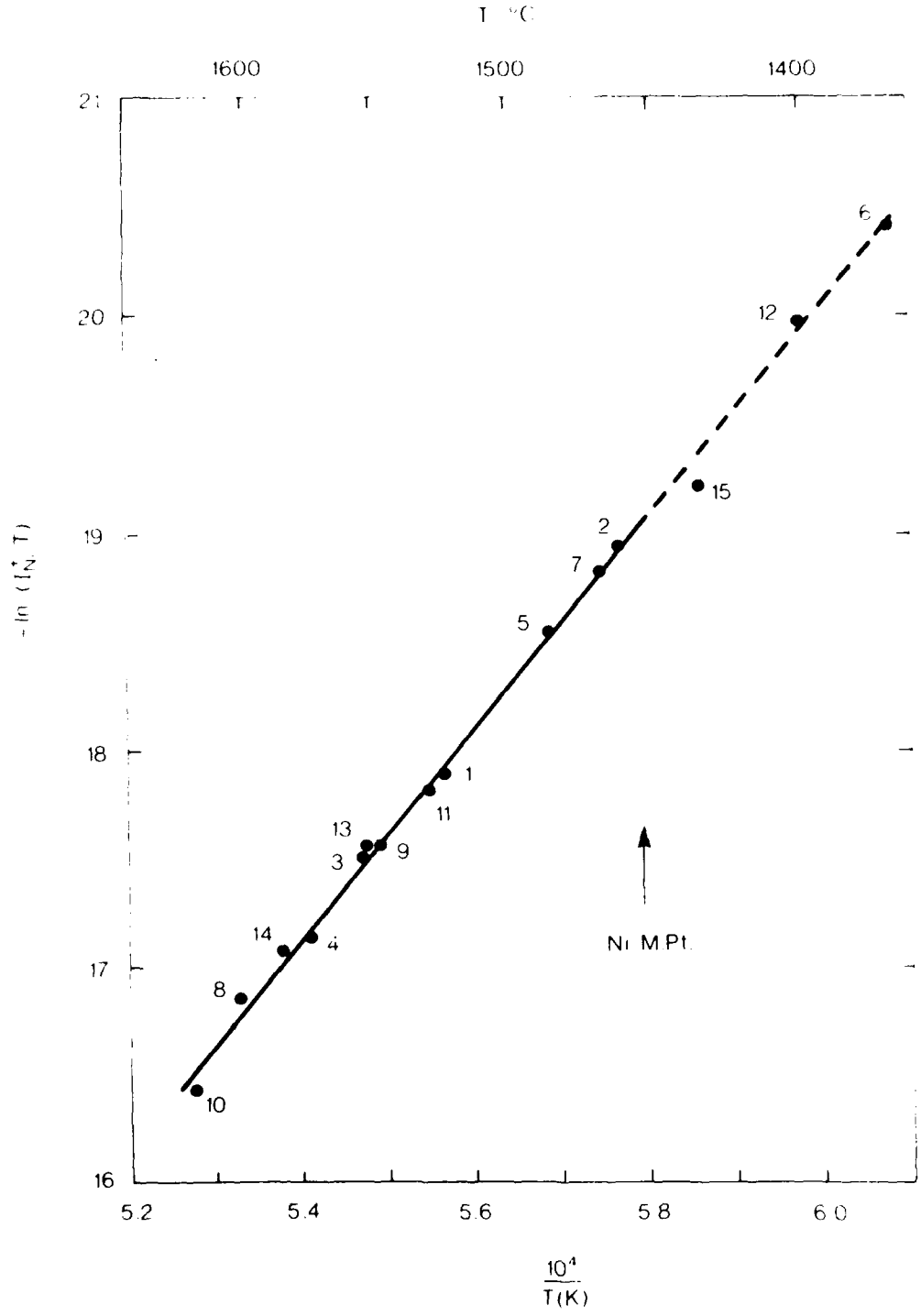

FIG. 16. Second-law plot for nickel vaporized from an alumina crucible in a molybdenum quad-cell. Ionizing electron energy 35 eV.

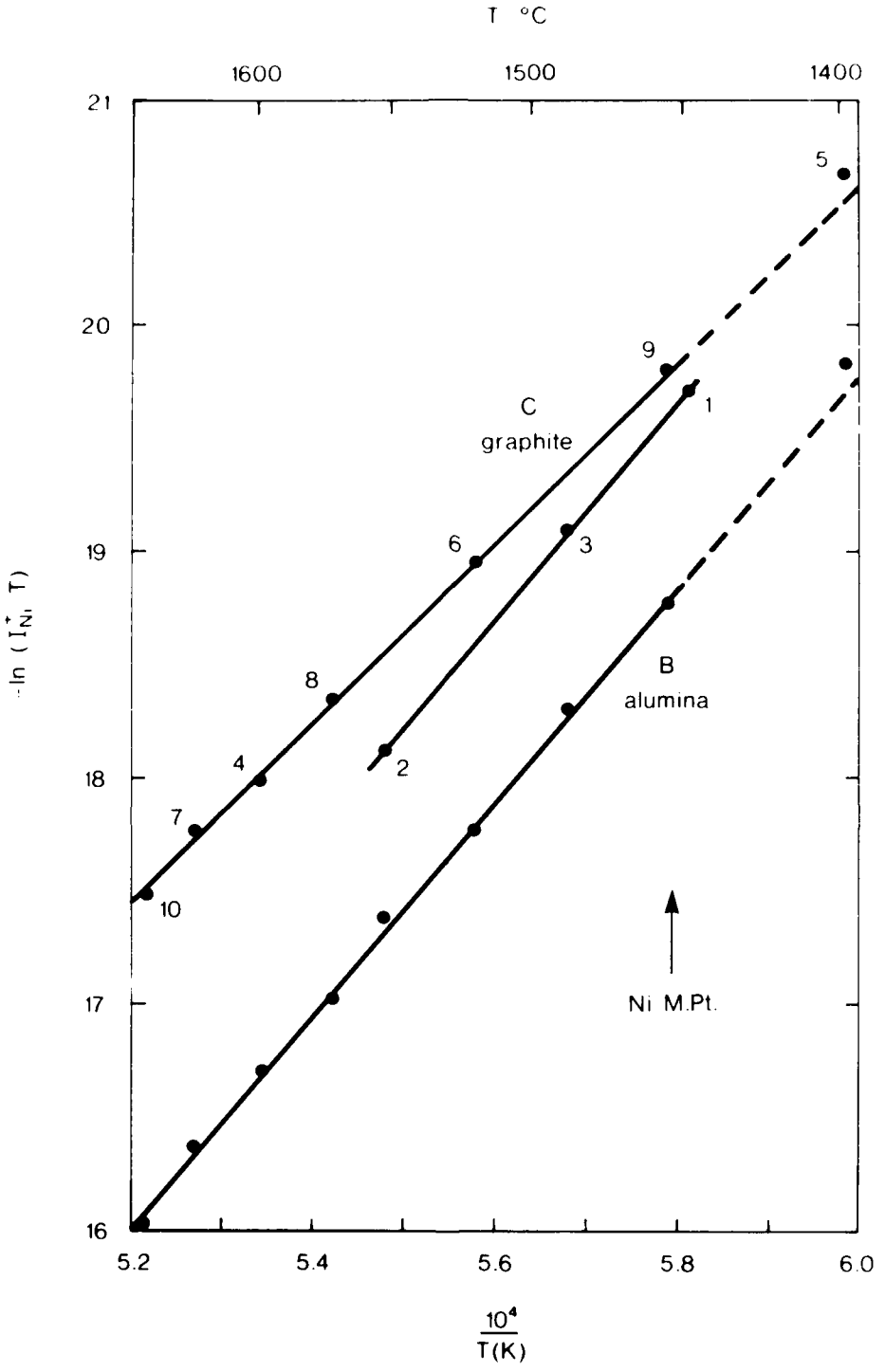

FIG. 17. Second-law plots for nickel vaporized from graphite (C) and alumina (B) crucibles in a molybdenum quad-cell. Ionizing electron energy 35 eV.

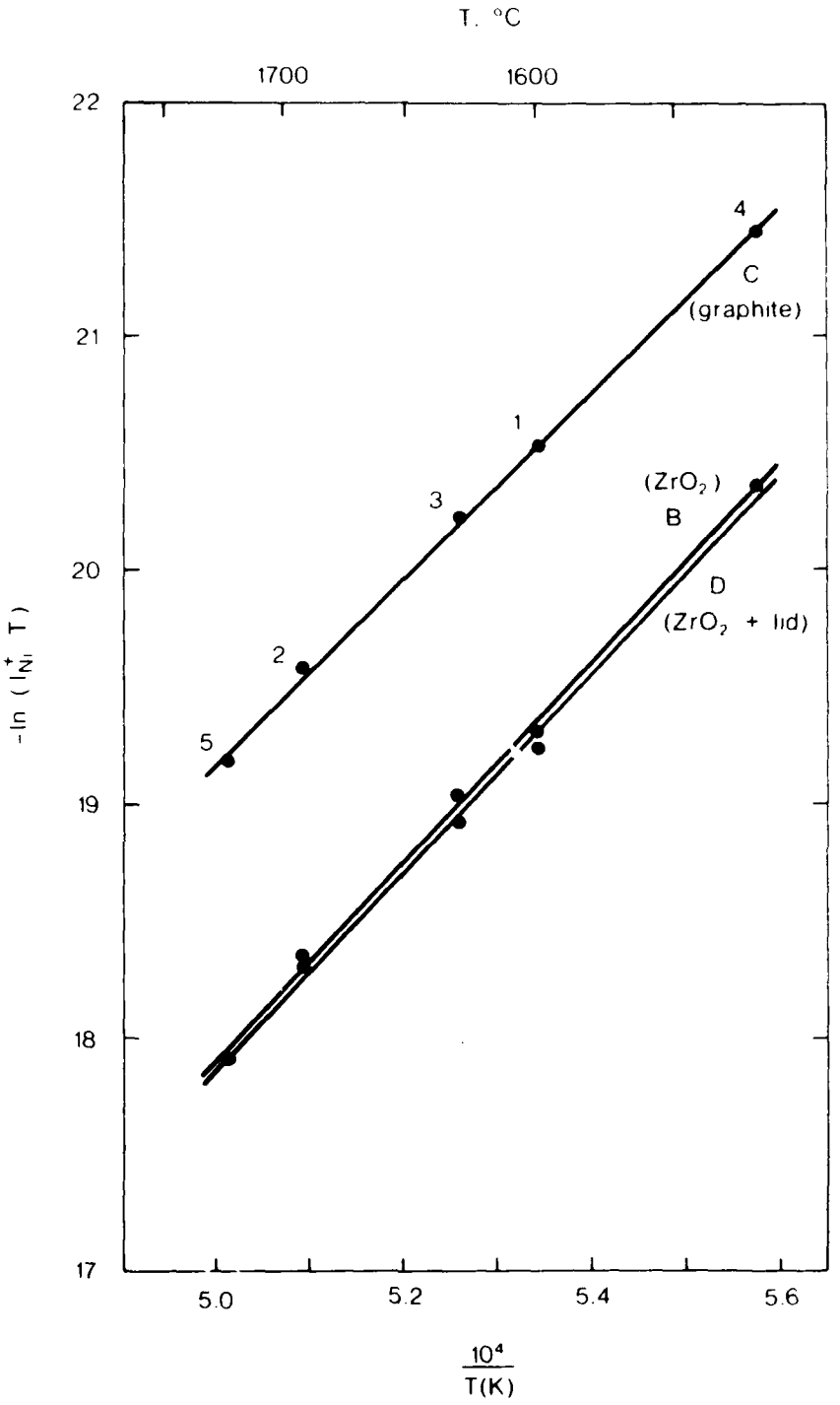

FIG. 18. Second-law plots for nickel vaporized from graphite (C) and zirconia (B and D) crucibles in a graphite quad-cell. D with zirconia lid, B without. Ionizing electron energy 35 eV.

DISTRIBUTION LIST

MATERIALS RESEARCH LABORATORIES

Director
Superintendent, Metallurgy Division
Dr G.R. Johnston
Library (2 copies)
Peter L. Mart

DEPARTMENT OF DEFENCE

Chief Defence Scientist (for CDS/DCDS/CPAS/CERPAS) (1 copy)
Army Scientific Adviser
Air Force Scientific Adviser
Navy Scientific Adviser
Officer-in-Charge, Document Exchange Centre (17 copies)
Technical Reports Centre, Defence Central Library
Director of Quality Assurance Support (DQAS)
Deputy Director, Scientific and Technical Intelligence
Joint Intelligence Organisation
Librarian, Bridges Library
Librarian, Engineering Development Establishment
Defence Science Adviser, Australia High (Summary Sheets Only)
Commission, London
Counsellor Defence Science, Washington, D.C. (Summary Sheets Only)
Librarian (Through Officer-in-Charge), Materials Testing Laboratories,
Alexandria, NSW
Senior Librarian, Aeronautical Research Laboratories
Senior Librarian, Defence Research Centre, Salisbury, SA

DEPARTMENT OF DEFENCE SUPPORT

Deputy Secretary, DDS
Head of Staff, British Defence Research & Supply Staff (Aust.)

OTHER FEDERAL AND STATE DEPARTMENTS AND INSTRUMENTALITIES

NASA Canberra Office, Woden, ACT
The Chief Librarian, Central Library, CSIRO
Library, Australian Atomic Energy Commission Research Establishment

MISCELLANEOUS - AUSTRALIA

Librarian, State Library of NSW, Sydney NSW
University of Tasmania, Morris Miller Lib., Hobart, Tas.

DISTRIBUTION LIST
(continued)

MISCELLANEOUS

Library - Exchange Desk, National Bureau of Standards, USA
UK/USA/CAN/NZ ABCA Armies Standardisation Representative (4 copies)
Director, Defence Research Centre, Kuala Lumpur, Malaysia
Exchange Section, British Library, Lending Division, UK
Periodicals Recording Section, Science Reference Library,
British Library, UK
Library, Chemical Abstracts Service
INSPEC: Acquisition Section, Institute of Electrical Engineers, UK
Engineering Societies Library, USA
Aeromedical Library, Brooks Air Force Base, Texas, USA
Documents Librarian, The Centre for Research Libraries, Chicago, Ill.
Defense Attache, Australian Embassy, Bangkok, Thailand


ATE
LME